

Information dynamics efficiently discriminates high γ -rhythms in EEG brain waves

Gustavo Menesse^{1,2*} Joaquín J. Torres¹

¹Department of Electromagnetism and Physics of the Matter and Institute Carlos I for Theoretical and Computational Physics, University of Granada, Granada, Spain.

²Departamento de Física, Facultad de Ciencias Exactas y Naturales, Universidad Nacional de Asunción, Paraguay

Abstract

The link between electroencephalography (EEG) rhythms, brain functions, and behavioral correlates is well established in the literature, and some of the physiological mechanisms of rhythm generation are also understood. However, discriminating between physiological waves, which can be linked to functional brain properties, and pathological waves, signatures of brain malfunction, is still problematic, especially in the case of high-frequency oscillations (HFO), such as high γ waves. Complex neuronal activity and rhythms typically observed in EEG recordings can also be observed in excitatory/inhibitory (E/I) NN models. Therefore, theoretical models present an opportunity to study the relationship between waves and neuronal circuit functions, which could lead to fundamental insights to discriminating waves. To try to address this and other questions, we explore here the emergence of high γ rhythms in an E/I balanced neural population of leaky integrated and fire neurons that includes short-term synaptic plasticity in the synapses. Although simple, this model generates a rich repertoire of EEG-like rhythms, including high-frequency excitatory and inhibitory oscillations not yet described in the previous related works. Using the integrated information decomposition framework (Φ -ID), we explore the information dynamics of the network and its relationship with excitatory and inhibitory activity and high-frequency rhythms. Our study shows that, in regions where high γ rhythms emerge only in the excitatory population, the informational properties observed in the network are more favorable for computation and processing information, corresponding then to functional regimes. However, regions where high γ rhythms also emerge in the inhibitory population present lower mutual information in general, which means that the system becomes less predictable, i.e., more random, a fact that can be linked to a less functional or "pathological" regime. Interestingly, in the second case, we also observe that both excitatory and inhibitory populations oscillate with the same dominant frequency, which is higher than in the first case. Higher frequency oscillations and synchronization are commonly associated with epileptic seizures; therefore, our results suggest that adopting an information dynamics approach could help differentiate between high-frequency oscillations related to cognitive functions from those related to neuronal disorders such as epilepsy.

Keywords: EEG, high frequency oscillations, neuronal networks, information dynamics.

Contents

1	Introduction	2
2	Model and Methods	4
2.1	Integrated information decomposition (Φ -ID) framework	4
2.2	EEG brain rhythms model	7
3	Results	11
3.1	Phase diagram, rhythms and information dynamics	11
3.1.1	Excitatory and inhibitory activity	11
3.1.2	Dominant rhythms for relevant regions of the phase diagram	11
3.1.3	Phase diagram and information measures	13
3.2	High frequency oscillations in EI high activity phase.	16
3.3	Information dynamics in the high γ oscillations regimes.	17
3.4	Limitations of our analysis from experimental point of view	21

1 Introduction

Non-invasive EEG exploration on the cerebral cortex has become a relatively simple, convenient and inexpensive way of analyzing consequences of how large populations of neurons can cooperate to develop complex brain functions while variations of their synaptic relations occur [35, 37, 54, 67]. In fact, EEG is a technique that allows one to easily visualize spontaneous brain activity organized in terms of waves or "rhythms" emerging due to the synchronization of millions of cortical neurons with main frequencies ranging from 0.5 to 35 Hz and more defining the so called δ , θ , α , β and γ bands. Moreover, each one of these rhythms are loosely associated with different states of consciousness, such as deep sleep, anesthesia, coma, relax, and attention, and with different mental and cognitive processes that the brain can perform [12].

The in-depth analysis of EEG time series has traditionally been shown to be a very useful tool to detect neurological disorders, such as epilepsy [55] and its association with autism spectrum disorder (ASD) [50] and it could also be useful to detect Alzheimer's disease (AD) in its early stages [16] and other brain pathologies. In particular, in the last years EEG data have regained significance thanks to the recent development of specific Machine Learning and Deep Learning techniques that use such data for high-accuracy detection and diagnosis of a broad range of such neuropathologies [21].

Among the variety of brain rhythms, those characterized by high oscillation frequencies (HFOs) are particularly intriguing and recently have attracted the attention of the scientific community because they are often associated with epileptic seizures [5, 47, 48], but at the same time there is also a relationship between HFOs and high cognitive functions [31, 52, 68]. The dichotomy between physiological HFOs, related to cognitive functions, and pathological HFOs is an important issue for the clinical analysis of EEG and electrocorticography (ECoG) [5] and exemplifies the complexity of understanding how rhythms and brain functions are related.

Generally, the HFO called the γ band goes from 30-150Hz. These are the oscillations that are usually related to cognitive functions [17, 52]. However, it is still debated whether these oscillations, in fact, implement a causal mechanism of brain functions or are instead a general dynamic mode of the neural circuit as suggested by [17]. Higher frequency oscillations, in general $> 150Hz$, are commonly used as epileptic seizures biomarkers [19, 47]. These HFOs are usually classified as ripples (100-200 Hz) and fast ripples (200-500Hz) [39, 48]. Some literature also propose ultra fast ripples ($> 500Hz$) as better epileptogenic zone biomarkers than lower frequency ripples [9].

The researchers tried to differentiate physiological from pathological HFOs by studying the properties of the oscillations, which means measuring frequencies, spectral amplitudes, and typical duration. However, this seems not helpful and even leads to contradictory results, as was addressed by the authors of [46], who presented an overview of studies comparing duration, frequency, and amplitude of presumed physiological and pathological ripples. To exemplify these contradictions in the recent literature, it suffices to cite two recent works; the first [19] where the authors found that pathological HFOs have a higher mean spectral amplitude, a longer mean duration, and a lower mean frequency than physiologically induced HFO, and a second and more recent article [46], in which exactly opposite properties of HFOs were found for each case. Mooij *et al.* [46] find higher precision in differentiating physiological from pathological HFOs when focusing on the co-occurrence of other phenomena, such as vertex waves and interictal epileptiform discharges, instead of only measuring properties of HFOs. However, there is still work to be done.

In general, dealing with real EEG data is a complex task that requires special expertise in signal analysis and noise reduction to prevent misinterpretation [5]. Therefore, modeling brain rhythms can be a simpler way to explore innovative EEG analysis techniques and perform a preliminary evaluation of the hypothesis on the mechanisms and functions behind different brain rhythms.

Some of the first and simplest models of EEG data were presented by [14], using an excitatory/inhibitory network of integrated and fire neurons that was able to generate alpha rhythms and their statistics similar to what is observed in the thalamus. In the recent literature, a reformulation of this model in terms of differential equations shows that the emergence of a variety of other rhythms and modulation between them can be observed in this model in terms of a few relevant parameters. Moreover, the complex phenomenology observed in a simple model can be understood through concepts of statistical physics and

dynamical systems theory, such as phase transitions, bifurcations, metastability and stochastic resonance phenomena [20, 51].

The dynamical systems/statistical physics approach has been demonstrated to be powerful and helps explain some aspects of complex systems behavior. However, it will not always give us a complete picture. More often, knowing the properties of a dynamical regime does not necessarily give us enough information about the "function" (in the biological sense) of a given dynamical phenomenon. Complementing this dynamical knowledge with the "information dynamics" [32] of a system gives us a more broad vision of what the system is doing and what possible functions could be favored by a given dynamical regime. For example, dynamical regimes with high redundancy information processing will be robust to failures and, therefore, could be linked to vital functions in an organism, as found for structurally coupled modular sensory-motor processing in the brain [34]. In addition, measuring the transfer of information between parts of a dynamical system allows us to define an effective connectivity network and provides a hint about the functional structure of a system [25]. On the other hand, a high integrated information regime has recently been related to the concept of criticality in the neural system [4], a condition that possesses a set of advantageous properties for efficient computing and information processing.

In recent years, the development of tools such as local information dynamics (LID) [32] and partial information decomposition (PID) [8] helps to extend our understanding of complex systems. More precisely, LID studies how a complex system locally stores, transfers, and modifies information; while PID analyzes the information between three random variables (two sources and one target) by decomposing it into three types of information "atoms": unique, redundant, and synergistic, each of which captures different fundamental relations between random variables. In this context, a framework called *Integrated information decomposition* (Φ -ID) was recently developed [33, 53]. Φ -ID seems capable of providing general insights of the dynamics and information content of very distinct dynamical systems, from cellular automata to networks of Kuramoto oscillators [41].

In the present work, we explore the emergence of coherent rhythms in a similar EEG model, approaching it not just by typical statistical physics and nonlinear dynamical points of view, but focusing on new information theory techniques, specifically integrated information decomposition (Φ -ID). Our goal was to understand the relationship between rhythm emergence and local information content and dynamics, looking for insights that help us differentiate rhythms by their informational content and the dynamical regimes where they emerge.

As main results, we first show that HFO rhythms emerge in a specific region of the phase diagram of an EEG model, which were not explored in previous literature. Combining the typical statistical physics approach of defining order parameters (which are global quantities) with the local information dynamics of the neuronal network, we found that the HFOs in different neuronal populations have fundamentally different information dynamical properties.

Specifically, we found that the γ_{High} band power density of regimes where excitatory and inhibitory HFOs have different frequencies with lower frequency of the excitatory ones, are related to an increase in redundancy in inhibitory information dynamics while maintaining the differentiation in excitatory information dynamics. Combining both differentiation and redundancy, we can say that in these regimes, the system is more capable of robust parallel processing of information; therefore, these HFOs are more likely to be functional, as physiological HFOs described in the literature [23, 31, 46]. On the other hand, we also found that when HFOs emerge with high power in both populations with the same frequency, information measures in the inhibitory group of neurons are lower, in general, which indicates less functional dynamics that could be related to pathological states.

From the neuroscience point of view, an analysis like the one done here, when applied to experimental data in combination with models, could help researchers differentiate brain states, regions, and functions. These tools can be applied to the decomposition of functional interactions between brain regions to reveal differences in information processing functions [34]. Also, as done in the present work, information dynamics analysis could point out relations between microscopic activity of a specific neuronal population, local information processing, and emergent macroscopic phenomena in a more or less straightforward way. For example, it can help to understand how different physiological mechanisms acting locally, such as short-term synaptic plasticity, neuronal adaptation, and other factors such as the underlying topology [60][44] and the existence of high-order interactions in the system[63][45][22], relate to emerging brain waves.

From the physics of complex systems point of view, our work here is an example of how information dynamics analysis through tools such as Φ -ID can provide insight about the emerging behavior, capturing details about dynamical phases and collective phenomena, which are complementary to those acquired by tools of statistical physics and nonlinear dynamics. Specifically, in our model, we found a relation

between the onset of a second-order phase transition in the form of a low-activity intermediate (LAI) transition [10] towards a maximum in integrated information. This and other relations between phase transitions and information dynamics will be explored in depth in future works.

2 Model and Methods

2.1 Integrated information decomposition (Φ -ID) framework

Before discussing the framework used to describe the information dynamics, we must clarify that here we refer to information as stated in the context of classical Shannon Information Theory, where information has a probabilistic definition, defined as the surprise $h(x_i)$ [13] produced by observing a state x_i of a random variable X given a state probability distribution $\mathcal{P}(x_i)$. The average of the surprise (information) is called the Shannon entropy H and can be viewed as a measure of ‘‘uncertainty’’ related to a random variable X states. All the information quantities in this article are presented in bits.

In the context of classical Shannon information theory, Φ -ID is a multivariate extension of Partial Information Decomposition (PID) [8], which gives us a unified framework to explore the information dynamics of a system through combinations of different information atoms. This framework proposes to capture how information in a system flows from present to future by decomposing the time-delayed mutual information (TDMI) into information atoms which, differently from PID, can manage multivariate sources and targets.

Frameworks like Φ -ID are interesting in the context of complex systems in general, a neuronal system in particular, because they can reveal emergent and higher-order interactions within the dynamics of a neuronal system [34]. For example, it can be applied in the decomposition of spontaneous spiking activity recorded from dissociated neural cultures to show how different modes of information processing are distributed over the system [66], and in our case how different modes of information processing are distributed over the phase space of a computational model.

While TDMI captures the information that past states give us about the future and vice versa, Φ -ID proposes to decompose mutual information as a sum of atoms of information I_∂ . We first need to separate our system into partitions and then study the information that the present (state at time t) of each partition provides about the future (state at time $t + \tau$) of itself, the other partitions, and the whole system.

In the simplest case, we have a bipartition \mathcal{B} with parts \mathbf{X}^1 and \mathbf{X}^2 , and we build an ordered set $\mathcal{A} = \{\{\{\mathbf{X}^1\}\{\mathbf{X}^2\}\}, \{\mathbf{X}^1\}, \{\mathbf{X}^2\}, \{\mathbf{X}^1\mathbf{X}^2\}\}$, which is called a redundancy lattice (more details of its mathematical properties are presented in [8, 40]).

Each element of this lattice represents a type of PID atom; the first element $\{\{\mathbf{X}^1\}\{\mathbf{X}^2\}\}$ is at the bottom of the redundancy lattice and represents the information carried by both parts redundantly, usually represented as **Red**. The second and third elements are related to the information carried uniquely by the respective part, usually symbolized by \mathbf{U}^1 and \mathbf{U}^2 . The last element is the information that is only accessible when both parts are considered together, which means synergistic information, and is commonly represented as **Syn**.

Now, if we consider the time evolution of these α PID information atoms, we have another equivalent lattice with four β PID atoms as shown in 1. Finally, the resulting redundancy lattice is the product between both $(\mathcal{A}_t \times \mathcal{A}_{t+\tau})$, giving us a set of 16 composed atoms of $\alpha \rightarrow \beta$. This means information atoms that were originally carried as a α atom (carried uniquely, redundantly, or synergistically), which in the future will be carried as β atoms. That said, mutual information is decomposed as

$$I(\mathbf{X}_t, \mathbf{X}_{t+\tau}) = \sum_{\alpha, \beta \in \mathcal{A} \times \mathcal{A}} I_\partial^{\alpha \rightarrow \beta}. \quad (1)$$

Each information atom $I_\partial^{\alpha \rightarrow \beta}$ is defined via a double redundancy function, namely $I_\cap^{\alpha \rightarrow \beta}$, and the sum of every atom that satisfies the ordering relation $\alpha' \rightarrow \beta' \preceq \alpha \rightarrow \beta$. The ordering relation \preceq is formally defined as $\forall \alpha, \beta \in \mathcal{A}, \alpha \preceq \beta \iff \forall b \in \beta, \exists a \in \alpha, a \subseteq b$. Therefore, the ordering relation of the *product lattice* $\alpha' \rightarrow \beta' \preceq \alpha \rightarrow \beta$ means that $\alpha' \preceq \alpha$ and $\beta' \preceq \beta$. All atoms in the sum have the same or less redundant information as the computed atom. Then, we write

$$I_\partial^{\alpha \rightarrow \beta} = I_\cap^{\alpha \rightarrow \beta} - \sum_{\alpha' \rightarrow \beta' \prec \alpha \rightarrow \beta} I_\partial^{\alpha' \rightarrow \beta'}. \quad (2)$$

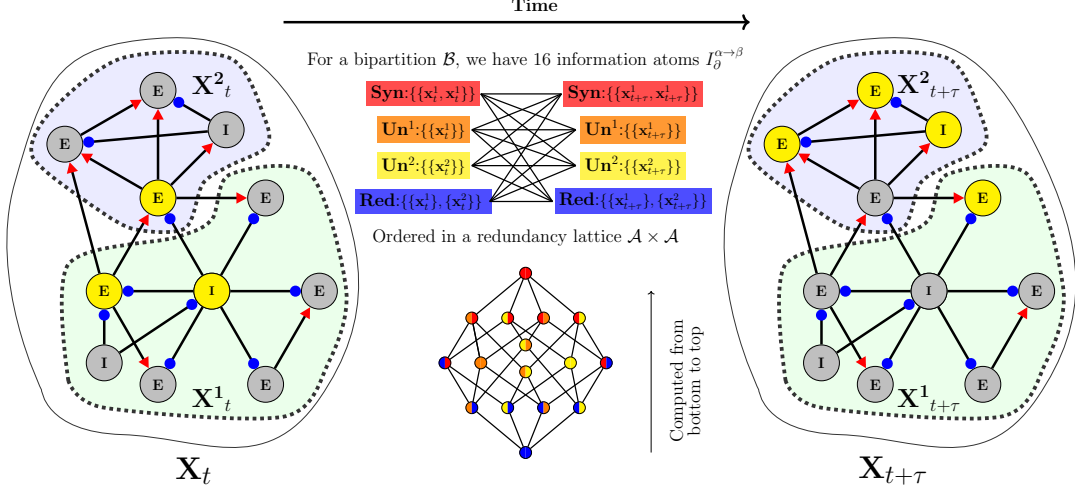


Figure 1: **Integrated information decomposition framework (Φ -ID)**. Although time-delayed mutual information quantifies how knowing a current state \mathbf{x}_t of our system reduces the uncertainty we have about future states $\mathbf{X}_{t+\tau}$ and vice versa, Φ -ID help us answer the question of how this information (uncertainty reduction) is carried by our system and how it changes from the present state to the future state (information dynamics). Given a partition of our system, in the simplest case, i.e. a bipartition, and after defining a redundancy and double redundancy function, all information atoms can be computed, following the redundancy lattice from bottom to top.

Now, for computing the atoms, we need to define a double redundancy function $I_{\cap}^{\alpha \rightarrow \beta}$. By following the axiomatic restrictions presented in the original formulation of Φ -ID [40], if $\alpha = \{a_1, a_2, \dots, a_J\}$ and $\beta = \{b_1, b_2, \dots, b_K\}$ with $\alpha, \beta \in \mathcal{A}$ and α_j, β_k non-empty subsets of $\{1, \dots, N\}$, this function can be reduce to PID redundancies, as

$$I_{\cap}^{\alpha \rightarrow \beta} = \begin{cases} \mathbf{Red}(\mathbf{X}_t^{a_1}, \dots, \mathbf{X}_t^{a_J}; \mathbf{X}_{t+\tau}^{b_1}) & \text{if } K = 1 \\ \mathbf{Red}(\mathbf{X}_{t+\tau}^{b_1}, \dots, \mathbf{X}_{t+\tau}^{b_K}; \mathbf{X}_t^{a_1}) & \text{if } J = 1 \\ I(\mathbf{X}_t^{a_1}, \mathbf{X}_{t+\tau}^{b_1}) & \text{if } J = K = 1. \end{cases} \quad (3)$$

This let us with the responsibility of choosing wisely a PID redundancy function \mathbf{Red} and a double redundancy function $\mathbf{Red} \rightarrow \mathbf{Red}$. There is no consensus on a universally preferable redundancy function, as this is still a work in progress [40, 53].

In the present work, for simplicity and to maintain a computationally tractable analysis, we only explore bipartitions of our system and use mutual minimum information (MMI) as redundancy and double redundancy functions. For a two-part system \mathbf{X}_i and \mathbf{X}_j , we have,

$$\mathbf{Red}(\mathbf{X}_t^{a_1}, \dots, \mathbf{X}_t^{a_J}; \mathbf{X}_{t+\tau}^{b_1}) = \min_i I(\mathbf{X}_t^{a_i}; \mathbf{X}_{t+\tau}^{b_1}), \quad (4)$$

$$\mathbf{Red}(\mathbf{X}_{t+\tau}^{b_1}, \dots, \mathbf{X}_{t+\tau}^{b_K}; \mathbf{X}_t^{a_1}) = \min_j I(\mathbf{X}_t^{a_1}; \mathbf{X}_{t+\tau}^{b_j}), \quad (5)$$

and

$$I_{\cap}^{\mathbf{Red} \rightarrow \mathbf{Red}} = \min_{i,j} I(X^i; X^j). \quad (6)$$

Once a redundancy function is defined and after estimating the probability distributions of t and $t + \tau$ states of the system, the decomposition only requires solving a system of 16 linear equations [40], which is straightforward. A schematic representation of the framework is presented in Figure 1.

TDMI already can quantify the information that the past or present of the system provides about its future, but does not give us details about how this information is actually provided. For example, a system could depend mainly on the state of a specific group of neurons, which means that most of the measured TDMI is provided by the state of this group of neurons, which means that any failure or alteration in this group will dramatically alter our knowledge about the evolution of the system. Another possibility is that information is provided redundantly by many groups of neurons, which means that

any neuron or group of neurons provides the same information about the future; therefore, eliminating some of these groups will not affect our knowledge about the future. Finally, we can have a regime where the information about the future is obtained only by knowing the states of all groups of elements jointly, which is called synergistic information.

In general, we can make the following interpretation about how the TDMI is decomposed. If there are many groups that carry unique information, this system is a highly differentiated system (with specialized parts). If the system is redundancy-dominated, it will have a high robustness to failures; as many parts of the system carry the same information, which indicates that these parts should have the same function. Finally, a system that is synergistic dominant is a high-integrated system, where all parts work together to define the future states of the system.

To identify the different dynamic information regimes, we group the atoms into 3 measures. The first was the revised effective information φ^R , proposed by [33, 41], mathematically express as,

$$\varphi^R[\mathbf{X}, \tau, \mathcal{B}] = I(\mathbf{X}_t; \mathbf{X}_{t+\tau}) - \sum_{j=1}^2 I(\mathbf{X}_t^j; \mathbf{X}_{t+\tau}^j) + \min_{ij} I(\mathbf{X}_t^i; \mathbf{X}_{t+\tau}^j). \quad (7)$$

From the effective information, the revised integrated information is defined as the normalized effective information of minimum information partition (MIP),

$$\Phi^R[\mathbf{X}, \tau] = \varphi[\mathbf{X}, \tau, \mathcal{B}^{MIP}] \quad (8)$$

$$\mathcal{B}^{MIP} = \arg_{\mathcal{B}} \min \frac{\varphi^R[\mathbf{X}, \tau, \mathcal{B}]}{K(\mathcal{B})} \quad (9)$$

$$K(\mathcal{B}) = \min\{H(\mathbf{X}^1), H(\mathbf{X}^2)\}, \quad (10)$$

where K is a normalization factor equal to the minimum entropy between the partition entropies [6]. The revised effective information φ^R captures synergistic information plus the information that is transferred between parts of the system. While Φ^R seeks to quantify the degree to which parts of a system are working together as a whole (degree to which the whole is more than the parts).

Second, we measure the information that is uniquely carried by each partition across time, defined in this framework as

$$Un[\mathbf{X}, \tau, \mathcal{B}] = \sum_k^2 \left[I(\mathbf{X}_t^k; \mathbf{X}_{t+\tau}^k) - \min_i I(\mathbf{X}_t^k; \mathbf{X}_{t+\tau}^i) - \min_j I(\mathbf{X}_t^j; \mathbf{X}_{t+\tau}^k) + \min_{ij} I(\mathbf{X}_t^i; \mathbf{X}_{t+\tau}^j) \right]. \quad (11)$$

Following the same strategy as for integrated information, to quantify the degree of information carried uniquely by a system, we look for the bottleneck. We first normalize $Un[\mathbf{X}, \tau, \mathcal{B}]$ using the same $K(\mathcal{B})$, and then search the partition that minimizes this quantity,

$$\mathcal{U}[\mathbf{X}, \tau] = Un[\mathbf{X}, \tau, \mathcal{B}^{MUP}] \quad (12)$$

$$\mathcal{B}^{MUP} = \arg_{\mathcal{B}} \min \frac{Un[\mathbf{X}, \tau, \mathcal{B}]}{K(\mathcal{B})}. \quad (13)$$

As this unique information is conceptually the opposite of the integrated information, we will call it differentiated information.

Third, to quantify the degree of redundancy of our system, we define a non-synergistic redundancy (\mathcal{R}) measure adding all redundancy-related atoms that do not contain a synergistic component; here, to avoid negative values, we need to compensate for the double redundancy subtraction in each of the other redundancy-related atoms. This is done by adding it four times more, which yields to,

$$\text{NS-Red} = \min_{ij} I(\mathbf{X}_t^i; \mathbf{X}_{t+\tau}^j) + \sum_k^2 \left[\min_i I(\mathbf{X}_t^k; \mathbf{X}_{t+\tau}^i) + \min_j I(\mathbf{X}_t^j; \mathbf{X}_{t+\tau}^k) \right]. \quad (14)$$

We will define the redundant information as the minimum non-synergistic redundancy, define as

$$\mathcal{R}[\mathbf{X}, \tau] = \text{NS-Red}[\mathbf{X}, \tau, \mathcal{B}^{MRP}] \quad (15)$$

$$\mathcal{B}^{MRP} = \arg_{\mathcal{B}} \min \frac{\text{NS-Red}[\mathbf{X}, \tau, \mathcal{B}]}{K(\mathcal{B})}. \quad (16)$$

The atoms that make up each measure are indicated in Figure 2 using the redundancy lattice representation.

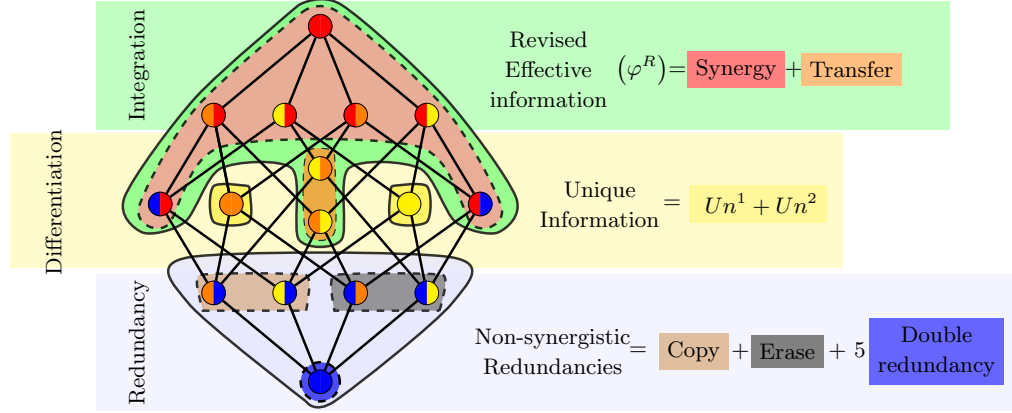


Figure 2: **Measures to capture information dynamics.** Information measures computed from information atoms presented in the redundancy lattice. Each node has two PID atoms from the present to the future ($\alpha \rightarrow \beta$) indicated by a color code: synergistic (red), unique 1 and 2 (orange and yellow) and redundant (blue). The colored area indicates the atoms that make up each measure. Revised integrated information [41] (green), unique information (yellow) and non-synergetic redundancies (blue).

2.2 EEG brain rhythms model

The model for generation of brain rhythms studied here was first introduced in [14] to reproduce EEG Alpha-rhythms obtained from activity recorded from the thalamus. Recently, the model was formalized and extended in [20] and [51] to study the emergent oscillatory response of a balanced E/I neural population to variable noisy inputs from other areas and explored the possibility of stochastic resonance phenomena and the relation between brain rhythm modulation and dynamic phase transitions. One of the main conclusions is that the model is capable of reproducing a variety of familiar brain rhythms in EEG recordings just by varying the level of noisy uncorrelated activity that arrives at the neural population of other areas [20]. Moreover, with the same model, in [51] it has been demonstrated the important role of short-term synaptic plasticity in induced explosive phase transitions from non-pathological to epileptic-like oscillatory behaviour.

Using a simple approach, the model considers two coupled regular two-dimensional networks with periodic boundary conditions (lattice on a torus). The first one, with N_E excitatory neurons disposed in a square lattice with c_E rows/columns and the second one with N_I inhibitory neurons disposed also in a square lattice with $c_I = \frac{c_E}{2}$ columns in a way that for each pair of excitatory columns, an inhibitory column fits in between, as shown in Figure 3. This model aims to capture the essentials of the cerebral cortex where excitatory where it is reported that neurons occur almost four times that the inhibitory ones [56], supposing to correspond this ratio to a balanced state of the cortex.

To coupling both lattices, each inhibitory neuron receives input from spikes arriving from the 32 adjacent presynaptic excitatory neurons and fires spikes which are input to 12 adjacent postsynaptic excitatory neurons, as shown in Figure 3. Following previous work [14, 20, 51], we consider only E-I and I-E interactions, since preliminary results including E-E and I-I connections seem not to significantly alter the dynamical phase space and emergent oscillatory behavior in the network [51].

Using the leaky integrated and fire neuron dynamic to monitor the time dependence of the membrane potential of each neuron, we describe the dynamics of the excitatory or inhibitory membrane potential $V^{E/I}$ as

$$\tau_m \frac{dV_i^E(t)}{dt} = V_r - V_i^E(t) + \frac{V_{min} - V_i^E(t)}{V_{min}} \sum_{m=1}^{K_I=3} V_{m=1}^{in,I}(t) + V^{noise}(t) \quad (17)$$

$$\tau_m \frac{dV_i^I(t)}{dt} = V_r - V_i^I(t) + \frac{V_{sat} - V_i^I(t)}{V_{sat}} \sum_{l=1}^{K_E=32} V_l^{in,E}(t), \quad (18)$$

where the factors $\frac{V_{sat} - V}{v_{sat}}$ and $\frac{V_{min} - V}{V_{min}}$ in the input terms were introduced to prevent physiologically

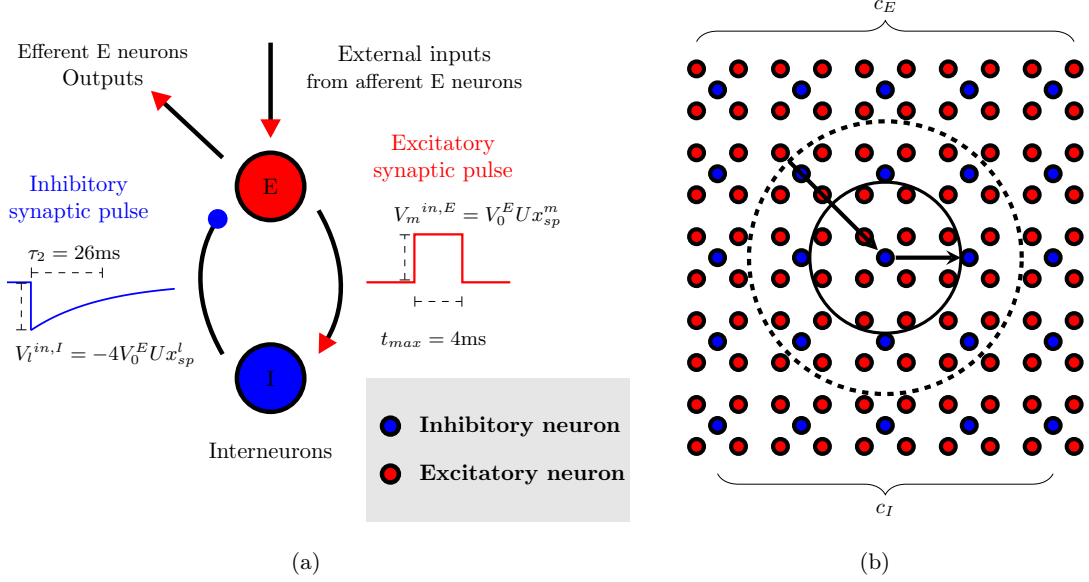


Figure 3: **Model for generation of EEG brain rhythms: Local dynamics and network topology.** (a) The model implements a minimal neuronal circuit, where excitatory and inhibitory pulses are different and act in different timescales. (b) Schemes representing the network topology used in the present study as in [14, 20, 51]. Inhibitory neurons (blue dots) have 32 pre-synaptic excitatory neighbors (red dots inside the dashed circle) while each of them are pre-synaptic neighbours of 12 excitatory neuron (inside the solid line circle).

unrealistic levels of membrane potential (too high or too low) around the resting membrane potential that it is set to $V_r = 0$. The limits used were $V_{sat} = 90\text{ mV}$ and $V_{min} = -20\text{ mV}$. Furthermore, the time constant τ_m is equal to $\tau_1(\tau_2)$ depending if the membrane cell voltage is above(below) the resting potential V_r [14]. The terms $V_\sigma^{in,I/E}$ $\sigma = m, l$ correspond to synaptic input coming from a neighbor presynaptic neuron when a spike takes place, which differs depending on the nature of the spike (excitatory or inhibitory), and follow the equations,

$$V_m^{in,I} = V_0^I U x_{t_{sp}} \Theta(t - t_{sp}) e^{-\frac{t-t_{sp}}{\tau_2}} \quad (19)$$

$$V_l^{in,E} = V_0^E U x_{t_{sp}} [\Theta(t - t_{sp}) - \Theta(t - t_{sp} - t_{max})], \quad (20)$$

where $V_0^{E/I}$ is the maximum amplitude of synaptic input, U is the release probability of neurotransmitter vesicles (viewed also as the fraction of resources released) and $x_{t_{sp}} = x(t_{sp})$ is the fraction of neurotransmitters available (which can be released) after the arrival of an action potential at time t_{sp} [65] (see below). In this model, excitatory spikes generate synaptic inputs in the form of square pulses of duration t_{max} , while inhibitory inputs generate pulses with exponential decay with decay time constant τ_2 [14].

The system is driven by a noise term V^{noise} which accounts for the excitatory inputs to E neurons from neurons in other regions of the brain. This noise is modeled assuming a lack of temporal correlations using a Poisson signal characterized by a noise level parameter μ . The noise level represents the mean value of external action potentials reaching each E neuron in 100 simulation time steps, which means that an E neuron receives on average $\lambda = \frac{\mu}{100}$ external spikes at each time step. In the simulations, we assume the existence of n external neurons so that the probability that each E neuron will receive an external spike from one external neuron is λ/n . Using a sufficiently large n , the external input per time has a Poissonian distribution. For all the simulations in this paper, we set $n = 100$.

We also account for the possibility of synaptic plasticity in the synapses and consider a simple mechanism of short-term depression (STD), in which synaptic efficacy, represented by the fraction of available neurotransmitters $x(t)$, decreases with the presynaptic firing rate due to the fast depletion of neurotransmitters inside the synaptic button and slow recovery after heavy presynaptic activity [64]. It has been

demonstrated that these STD mechanisms have strong computational implications in the functioning of different neural systems [61] such as an increase in memory capacity [42], optimal transmission of information in noisy environments[59][62], appearance of dynamical memories [58], etc. The STD mechanism is introduced by the equation

$$\frac{dx(t)}{dt} = \frac{1-x(t)}{\tau_{rec}} - Ux(t)\delta(t-t_{sp}), \quad (21)$$

with the delta function indicating that the second right-hand term occurs only for $t = t_{sp}$. For simplicity, concurrent mechanisms such as short-term synaptic facilitation [26] were not included.

The set of equations (17-21) describes the dynamics of the neuron membrane potential below a firing threshold, namely V_{th} , so when $V_i^{E/I} > V_{th}$ a spike is generated. Following previous work, to introduce the possibility of absolute (t_a) and relative refractory periods after the generation of voltage spikes at t_f , the firing threshold is considered to be time dependent following the time dependence

$$V_{th}(t) = \begin{cases} V_{th}^0 + (V_{sat} - V_{th}^0) e^{-\kappa(t-t_f-t_a)} & t_f < t < t_f + t_a \\ V_{sat} & t > t_f + t_a \end{cases}. \quad (22)$$

Here, when a spike takes place, the threshold is first set at V_{sat} during a period of t_a ms to prevent any further spike generation accounting for an absolute refractory period. Then it decays exponentially to its resting value V_{th}^0 with a time constant κ^{-1} that mimics the existence of a relative refractory period.

All parameters, symbols and values used in our study are summarized in Table 1. Throughout the text, we use the noise level μ and the recovery time constant τ_{rec} as the system control parameters, while all the other parameters were fixed. All differential equations in the model were numerically integrated using a simple first-order Euler method with time step $\Delta t = 4/100$ ms.

Table 1: Meaning, symbols and values of the EEG model parameters

Parameters	Symbols	Values
Depolarized membrane potential time constant	τ_1	16 ms
Hyper-polarized membrane potential time constant	τ_2	26 ms
Synaptic resource recovery time constant	τ_{rec}	0 to 300 ms
Proportion of synaptic resources released at each spike	U	0.5
Maximum excitatory input amplitude	V_0^E	10 mV
Maximum inhibitory input amplitude	V_0^I	-40 mV
Resting membrane potential	V_r	0 mV
Saturation membrane potential	V_{sat}	90 mV
Minimum allowed membrane potential	V_{min}	-20 mV
Excitatory pulse duration	t_{max}	4 ms
Firing membrane potential threshold	V_{th}^0	6 mV
Absolute refractory period	t_a	4 ms
Relative refractory period time constant	κ^{-1}	0.5 ms
Number of external neurons	n	100
Noise level	μ	0 to 15
Integration time step	Δt	0.04 ms

We have explored the dynamic phase space of the model by simulating 10^7 time steps for different values of τ_{rec} and μ , reproducing the results presented in [51] and obtaining the different dynamical regimes and phase transitions already reported. In all simulations, we used a network with $c_E = 14$ ($N_E = 196$) and $c_I = 7$ ($N_I = 49$). To monitor the emerging system rhythms, we define a local field potential (LFP) scheme, which consists of measuring the average membrane potential of the network by segmenting the network into 5 regions, as shown in Figure 3a. We selected groups of 32 E neurons and 9 I, computed the average membrane potential at each time step over the whole group of neurons, obtaining then a kind of LFP time series for excitatory and inhibitory neurons separately.

At fixed parameters τ_{rec} and μ , the obtained average membrane potentials over the neuron group or LFP are expected to be more or less stationary as the system reaches its stationary regime; therefore Fourier transforms should be enough to analyze the spectrum's of each LFP time series. Furthermore, taking LFP measures of excitatory and inhibitory populations separately allows us to explore the differences between rhythms in each population, analysis that will not be possible in experimental data.

Beyond the membrane potential, the time series of the spike trains for each neuron was also calculated by saving the state X of each neuron. The state is a Boolean variable $X = \{0, 1\}$, with 0 for inactive or silent neurons, and 1 for active or firing neurons. Time binning was applied to reduce the size of the time series and reduce the computational resources needed for the analysis. Considering that the absolute refractory period in this simulation is set to 100 time steps (4ms at $\Delta t = 4/100$ ms), the bin widths used were 100 steps. If a neuron spikes in that interval, the bin has value 1, otherwise its value was 0. These spike trains were used to study the information dynamics of the networks, as discrete variables are simpler to analyze with information theory tools.

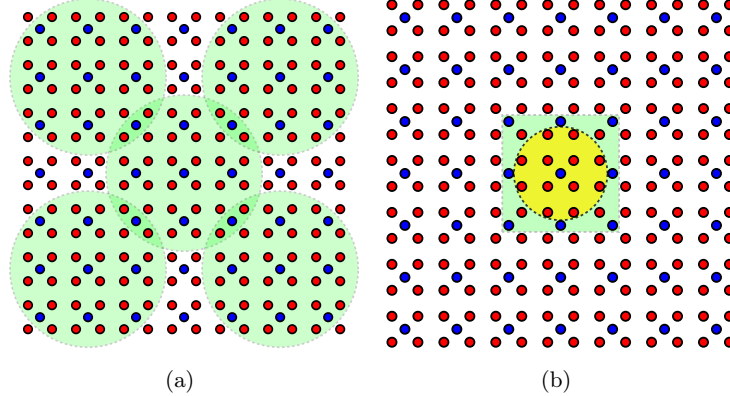


Figure 4: **Measurement schemes for study the information dynamics of the network.** (a) LPF-scheme: Five groups of 32 E and 9 I neurons (inside green circles) across the network were selected. The average membrane potential for each group was calculated, generating a five-channel EEG-like time series. (b) Scheme for Φ -ID analysis: 12 E neurons (E neurons inside the yellow circle) and 9 I (I neurons inside the green square) were selected. The states (active/inactive) of each of them were saved by obtaining a time series of discrete Boolean variables.

To explore the phase space, following the previous literature, we used the noise level μ and the recovery time τ_{rec} as a relevant control parameter. As the order parameter, we use the time average of excitatory and inhibitory network activity. This is defined as the proportion of active neurons (firing neurons) in a given time bin t , $\rho^E[t] = \frac{1}{N_E} \sum_i^{N_E} X_i[t]^E$ and $\rho^I[t] = \frac{1}{N_I} \sum_i^{N_I} X_i[t]^I$, where $X_i[t]$ is the Boolean state of a neuron in the time interval t (being 1 when the neuron fires in that time interval or 0 otherwise). Simulations of 800 seconds of network evolution were performed (2×10^7 time steps), which means that 2×10^5 time bins of 4 ms were obtained to compute the network activity statistics at each point in the space of explored parameters (μ, τ_{rec}).

To study the information dynamics of the model, we selected the central group of 12E and 9I neurons (as shown in Figure 3b) and saved the individual spike train of a group of neurons; this analysis in some sense considers only local interactions (interactions between first neighbors). It is worth mentioning that the topology used here does not facilitate long-range interactions, so observing an active information dynamics between distant neurons is less probable; nevertheless, it is an interesting complementary analysis to be explored in further work.

From the spike time series, we compute the probability of state distribution by counting the frequency of each state, first for the joint state at time t and $t + \tau$ of the E and I groups, $\mathbf{X}^E = \{x_1^E, \dots, x_{12}^E\}$ and $\mathbf{X}^I = \{x_1^I, \dots, x_9^I\}$, and second, for each possible bipartition of each group, $\mathbf{X}^{E,1} = \{x_1^E, \dots, x_s^E\}$ and $\mathbf{X}^{E,2} = \{x_{s+1}^E, \dots, x_{12}^E\}$ for the E group, and $\mathbf{X}^{I,1} = \{x_1^I, \dots, x_p^I\}$ and $\mathbf{X}^{I,2} = \{x_{p+1}^I, \dots, x_9^I\}$ for the I group. With these distributions, it was possible to compute the redundancies and, with them, all other information atoms. Having calculated the information atoms for each possible bipartition of our system, we can compute the revised integrated information Φ^R , the differentiated information \mathcal{U} and the non-synergistic redundant information \mathcal{R} as explained in the previous section.

3 Results

Although the main focus of the article is the analysis of γ waves in our model. We choose to first present a more complete picture of the phase diagram, rhythms, and information dynamics in our model and then focus our attention on Γ waves. The results section is organized first by presenting the phase diagram of the system given the neuronal activity as an order parameter (global measure). Second, we present the regions in the phase diagram where the different waves are dominant. Third, we show the different information measures obtained along the phase diagram. And finally we focus our attention on what these different approaches are telling us about the high-frequency oscillations on our model.

3.1 Phase diagram, rhythms and information dynamics

3.1.1 Excitatory and inhibitory activity

The phase diagram based on the neuronal activity of the system in the (μ, τ_{rec}) parameter space is shown in Figure 5.a. Three different regions are observed. First, with very low noise μ , to the left of the continuous transition (white solid line) we have a subcritical regime where both E and I neuron populations are inactive $\rho \approx 0$ (black region I). The second region (II) between the continuous phase transition and a discontinuous transition (white dashed line) is characterized by the fact that the E and I neuronal populations are both active, but they can be in different regimes: a low intermediate activity (II.a) and a high activity regime (II.b). Finally, we observe a third region (region III) after the discontinuous transition, where excitatory activity increases dramatically, while inhibitory activity dies off as the synaptic recovery time constant τ_{rec} is too large to allow an effective coupling between excitatory and inhibitory neurons.

We also measure the temporal variance of the activity of both neuronal populations (Figure 5.b). We found that excitatory populations have low variability in their activity, with the exception of a small region, whereas inhibitory populations show rich behavior in the high-activity region (II.b). This difference could be explained by the fact that excitatory activity is driven by the external noise and modulated/stabilized by inhibitory activity, while inhibitory activity depends only on excitatory activity and is not modulated, since I-I connections were not included. In future work, we will explore the impact of I-I and E-E connections in the activity fluctuations and in the information dynamics of this model.

In Figure 5.c, we observe the variance of the neuron states X instead of the temporal variance of neuronal activity ρ . We see that a maximum (gray region) occurs at the transition from low activity (II.a) to high activity (II.b), indicating that a phase transition could be taking place, a transition equivalent to the so-called low activity intermediate (LAI) phase transition [10].

In conclusion, from this analysis we observe that there is four characteristic regimes related to the network activity:

- I) Silent phase: An absorbing or silent regime for low external drive μ , which is almost independent on the time scale constant of the synaptic resources recovery τ_{rec} .
- II.a) LAI phase: A low activity intermediate region between the second order and first order transition lines, occurring for small to intermediate values of μ and τ_{rec} in both neuronal populations.
- II.b) High EI activity phase: A high activity region of both neuronal populations for high external noise μ and intermediate values of τ_{rec} ($50 \lesssim \tau_{rec} \leq 200$).
- III) Pure excitatory phase: After a critical value of τ_{rec} , the activity of the inhibitory population vanishes and a high excitatory activity driven by noise emerges.

Now we will explore the emergence of rhythms in the average membrane potential of excitatory and inhibitory neurons and relate them to the emerging phases described above.

3.1.2 Dominant rhythms for relevant regions of the phase diagram

The relation between specific rhythms and system dynamical phases can be important for understanding how particular rhythms in the brain can emerge in terms of some physiological information (for example, level of synaptic plasticity in some brain areas in our case) and therefore to relate some relevant physiological parameters with cognitive functions associated with those rhythms. With this aim, we track the main peaks of the power spectrum density of the system's average membrane potential time series in different frequency bands, across the space of the relevant parameters considered. The band

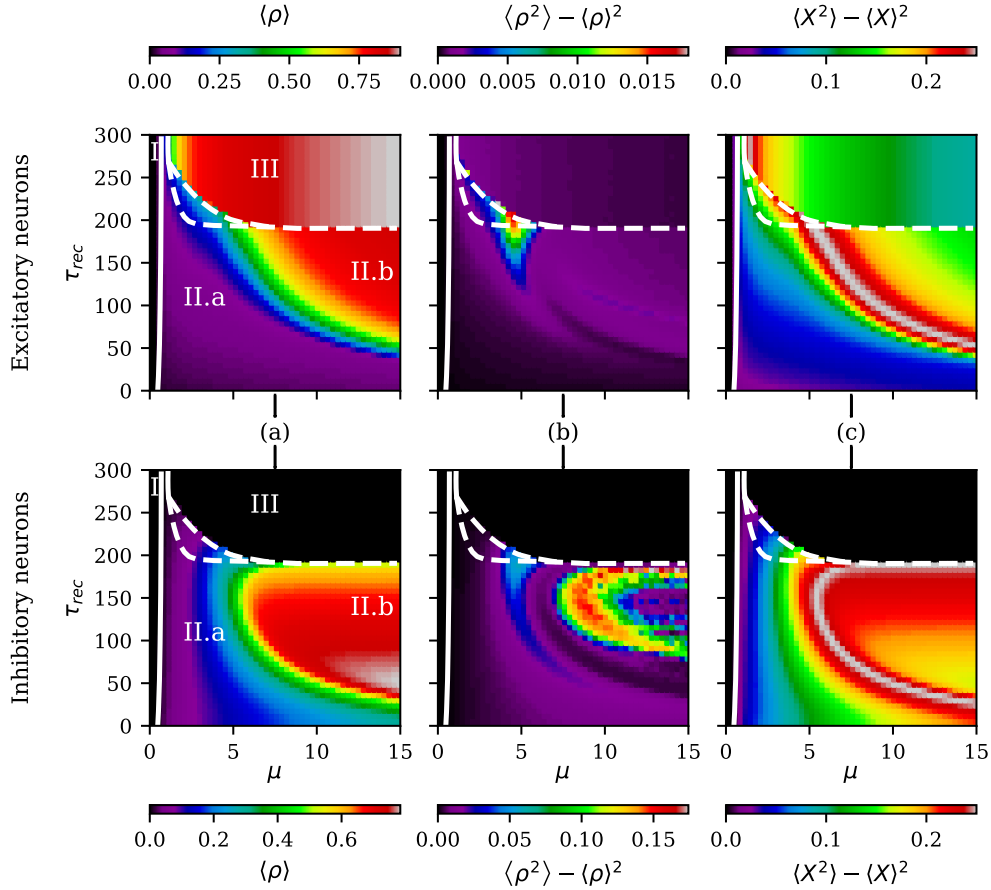


Figure 5: **Neuronal activity features across the (μ, τ_{rec}) parameter space.** The solid white line on the left shows the second-order phase transition from silent to active state (AT). The dashed white line shows the emergence of an explosive first-order transition. The region between dashed lines is the meta-stable phase, as described in [51]. (a) Temporal average of excitatory and inhibitory neuronal activity: The region between the second-order and first-order transitions shows what appears to be a low activity intermediate phase (II.a), which gives place to a full active phase of high activity (II.b) for noise values $\mu > 5$. (b) Temporal variance of excitatory and inhibitory neuronal activity: The inhibitory population shows a complex activity pattern, whereas the excitatory population has low temporal variability in activity. (c) Temporal variance of Boolean states (X) of neurons: The maximum variance (gray region) appears to mark the transition line between the low activity intermediate phase and the high activity phase.

classification we used was the following: $(0.5 - 3.5)Hz$ for δ , $(7.5 - 12.5)Hz$ for α , $(12.5 - 30.5)Hz$ for β , $(30.5 - 60.5)Hz$ for γ_{Low} and $> 60.5Hz$ for γ_{High} . Figure 6 shows a phase diagram indicating the areas where different rhythm bands appear in excitatory and inhibitory populations.

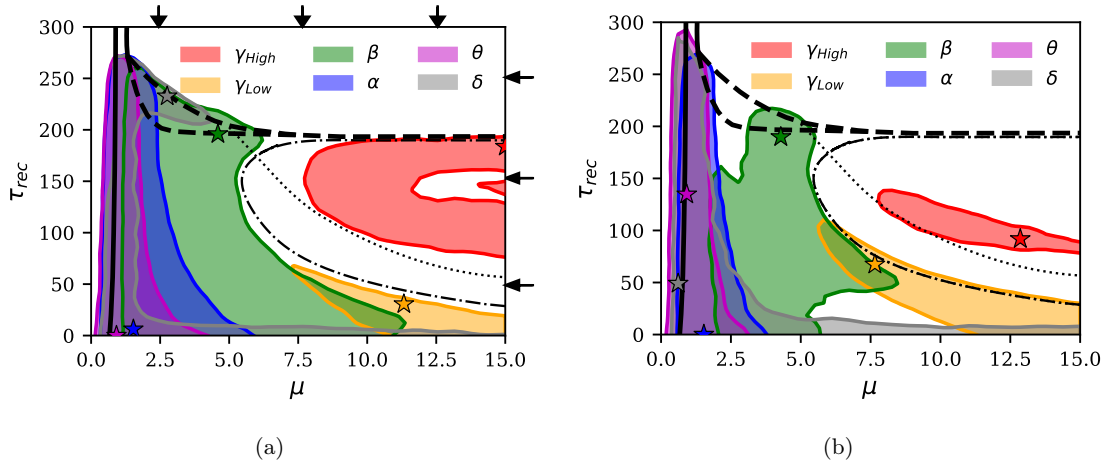


Figure 6: **Phase diagram of rhythms in the model.** Rhythms observed in the (a) excitatory and (b) inhibitory population across the phase diagram. Each color shows a specific band of brain rhythms. The regions were defined as the area of phase space where the maximum PSD in a given band is greater than 10^{11} , with the exception of γ_{Low} where the threshold was 10^{10} . The colored stars indicate the maximum of maxima for each rhythm. The detailed PSD for each band is presented in Figure ?? of the Supplementary Material. The solid line indicates a second-order phase transition (absorbing-active phase transition); dashed line indicates a first-order phase transition. Dotted and dash-dotted lines indicate, respectively, the onset of transition to a LAI phase, for the excitatory and inhibitory population.

The average membrane potential time series for each group of neurons at points of maximum power in different bands (colored stars in Figure 6) is shown in the Supplemental Material (Figures ?? and ??). We also present the power spectrum of both excitatory(inhibitory) average membrane potential time series at fixed values of $\tau_{rec}(\mu)$ in supplemental material Figure ?? (Figure ??). The fixed points used are indicated in Figure 6.a as black arrows.

Figure 6 shows that the low frequency rhythms emerge in a broad interval of synaptic recovery time scales but in a non-trivial manner. For example, as described in [51], $\delta - \beta$ modulations emerge in the metastable region (between first-order transition lines). But we also observe δ rhythms coexisting with other rhythms for low τ_{rec} depending on the intensity of external noise μ . The most relevant observation for this article is the emergence of excitatory and inhibitory HFOs (γ_{High}) in the high EI activity phase (II.b of Figure 5). These regions are shown as red areas in Figure 6, and will be the focus of analysis in the following sections. But first we will broadly explore the information dynamics of the whole phase diagram.

3.1.3 Phase diagram and information measures

We use the spiking train of excitatory and inhibitory neurons of the model to compute the three different information measures across the parameter space (μ, τ_{rec}) as explained above (see Model and Methods section). With such information measures we computed the phase diagrams presented in 7 together with the phase transitions already explained in previous sections (white solid and dashed lines).

Each of the information measures has a different behavior across the parameter space and between neuron populations. In region II.a, where low-frequency rhythms emerge in the excitatory population, the information is carried redundantly for large values of τ_{rec} (Figure 7.b top). These results suggest that the regions where low-frequency oscillations δ , θ and α are dominant are related to redundancy in excitatory population. Considering that redundancy may indicate robustness to failure, if we assume that the model captures some fundamental properties of brain oscillations, low-frequency waves could be associated with basal brain functions, which are the ones that requires more robustness [34]. However, from the functions usually associated with low-frequency waves, for example, memory consolidation and

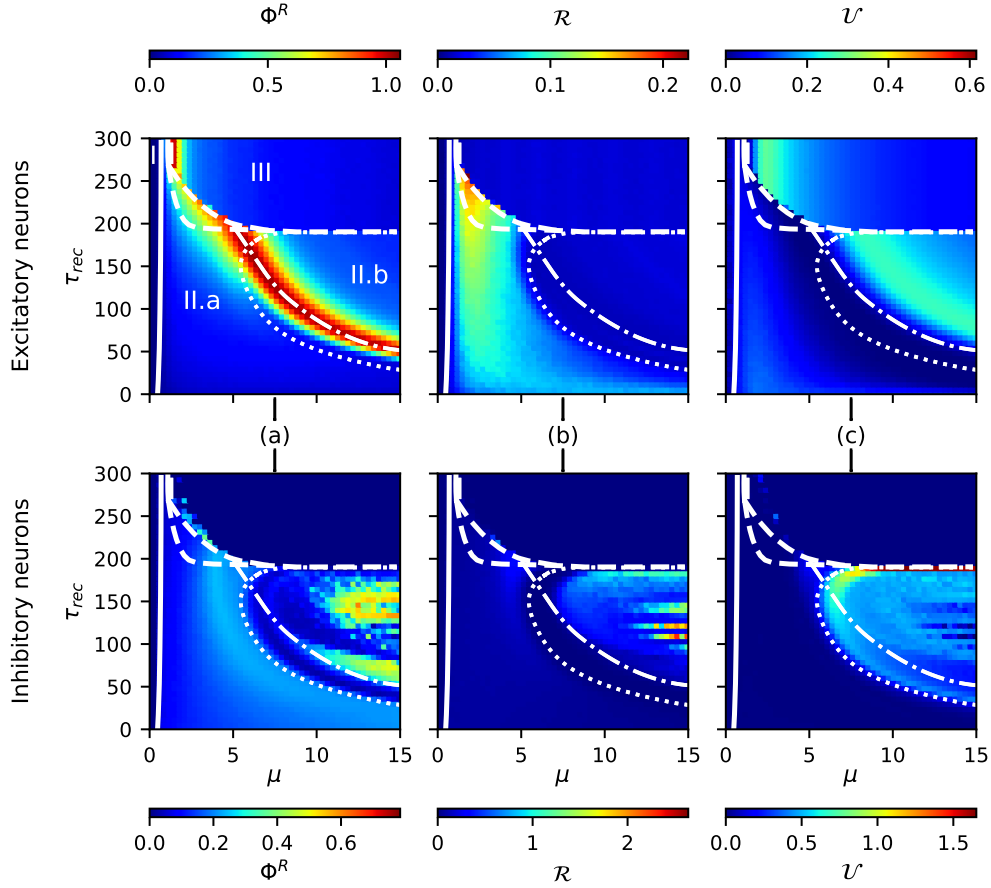


Figure 7: **Information dynamics across phase diagram for time delay $\tau = 1$ (4ms)**. The solid(dashed) white line describes the already explained above second-order(first-order) phase transition present in the system. The dotted (dash-dotted) white line indicates the maximum variance in the states of the I (E) neurons (see figure 5). Color code indicates Information measures level. (a) Integrated information in the excitatory group of 12E and the inhibitory group of 9I. (b) Redundant information in excitatory and inhibitory groups. (c) Differentiated information in excitatory and inhibitory groups. Measures made in a sub-population of neurons as indicated in Fig. 3b

deep NREM sleep related to δ [11], it is not easy to establish obvious connections between the information dynamic observed in this model and the actual brain function associated with low-frequency waves.

In the inhibitory population, close to the LAI-like phase transition (transition between II.a to II.b), we see that the integrated information is higher where β and γ_{Low} rhythms emerge, suggesting that these intermediate frequency rhythms are, in fact, a different phenomenon from the point of view of information dynamics. Higher integrated information indicates that the states of the network depend on the whole rather than parts (synergy) to define its dynamics. This higher synergistic regime is a property usually associated with higher-order and complex cognitive functions [2, 34]. At the same time, β and γ waves are also historically associated with "mental activity" [30]. Some of the functions usually attributed to these bands are [15, 30]: focusing action-selection network functions, decision making, and motor planning, activities that require higher states of awareness. Here, it is intriguing to see that the results observed in our model about the relation between β and γ_{Low} bands and higher Φ^R in the interneuronal population seem compatible with what should be expected for functions attributed to these waves.

Another interesting behavior is the maximization of excitatory integrated information in the LAI-like phase transition, which could be related to the effect of criticality over the information dynamics. In fact, it is already known that critical regimes were shown to be related to maximization in integrated information in simpler models, such as the Ising model [3] and the Kuramoto model [29, 41]. However, in such simple models, the maximum of Φ is related to a clear second-order transition, while in our case we are seeing something more close related to a LAI phase transition, which can be viewed as a disrupted second-order transition that appears in sparse topology when inhibitory elements are present [43]. This indicates that Φ^R can be sensible to criticality in general, even where exact critical points no longer exist.

In Figure 7.c (bottom), we observe that differentiated information has an abrupt peak in the inhibitory population over the first-order transition line from region II.b to region III, indicating that this dynamical transition has an information dynamics transition counterpart.

In SI (Figures ?? and ??), we present similar phase diagrams of information dynamics for Φ^R, \mathcal{R} and \mathcal{U} with other values of time delay τ ($\tau = 10$ and 100). We see that the maximum integrated information Φ^R is invariant on the explored time scales. Finding this time scale invariance in Φ^R is an interesting phenomenon that could be related to large time correlations in neuronal states. Large time correlations are expected in systems at some critical state [27], so if integrated information is related to criticality, as suggested by previous results in simpler models [1, 3, 29], our results show that Φ^R in the excitatory population may be an indicator of critical properties in a neuronal system. Moreover, Φ^R has an important additional feature since it seems to be sensitive to the LAI phase transition even when we measure Φ^R over a small population of neurons (12 neurons). Other common criticality identifiers, such as power laws in size and duration of neuronal avalanches, could not be properly measured in such a small population. Therefore, Φ^R could be a powerful tool to study criticality in actual neuronal networks.

Φ^R was proposed as an universal indicator of complexity [41]. At same time, critical phenomena such as avalanches following power laws distributions was related to maximization of complexity in a actual neuronal system [57]. However, our results shows that there is no need to have a well define second-order phase transition and critical points to maximize integrated information. It seems that a "relaxed" phase transition such as the LAI phase transition is enough. This could help to push forward the critical brain hypothesis.

In relation to the other two information measures, i.e. redundancy and differentiation (Figures ??b, ??c, ??b and ??c), in the excitatory group, we see a decrease in both measures as the time delay increases. This indicates that the excitatory information dynamics occurs at short time scales, with exception of the excitatory LAI phase transition. In the inhibitory population, however, both measures remain large but change in a complex manner with time delay, indicating a complex information dynamics between inhibitory neurons that spans over larger time scale, a fact which does not occur in the excitatory group.

In our system, inhibitory neurons are interneurons that modulate the activity of excitatory neurons. The fact that information dynamics is more complex for such inhibitory neurons is consistent with the role of interneurons. Interneurons are responsible for locally controlling neuronal circuits, through feed-backs with excitatory neurons, and for processing and transfer information in neuronal circuits [18, 36]. However, it is surprising to see that even dough in this model all interneurons are the same, a high complex behavior already emerges. This is mainly due to the introduction of short-term synaptic plasticity, a simple homeostatic mechanism which generates heterogeneity in the coupling strength between neurons and allows for a complex interplay between excitation and inhibition. This conclusion can be reached by noting that when such homeostatic mechanism is shut down ($\tau_{rec} \approx 0$), no complexity is observed

independently of the noise level μ .

The literature more often assumes that greater diversity in the type of neurons induces a large complexity of the information flow of the neuronal circuit, and at least two types of neurons, parvalbumin (PV) and somatostatin (SST), are often considered to explore this complexity [28]. But our model shows that even without diversity, interneurons could induce outstanding complex dynamics just by varying a few physiological parameters, which in our case are the short-term plasticity level and the external noisy inputs from afferent neurons.

One of the most interesting properties of this model is the emergence of high-frequency oscillations in both populations in a complex manner. Considering the current issues with differentiating pathological from physiological HFOs, we focus on studying these high-frequency oscillations in our model. The main goal was to understand how its relate with neuronal activity and, more specifically, to characterize the dynamical and informational properties of the system operation in regions of parameter space where these oscillations emerge.

3.2 High frequency oscillations in EI high activity phase.

In Figure 6 it can be seen that high γ oscillations ($> 60\text{Hz}$) emerge in the high activity phase in both populations, but inhibitory oscillations are only dominant ($\text{PSD} > 10^{10}$) in a restricted area, where they coexist with excitatory γ rhythms, just above the LAI-like transition in the excitatory population, in the so-called high EI activity phase (II.b).

To exemplify the emergence of high-frequency oscillations in the average membrane potential in this model, Figure 8 shows a time window of 1 second of the average membrane potential of 5 excitatory and inhibitory neurons groups (as indicated in Figure 4.a of Model and Methods section) at the points of the parameter space where excitatory and inhibitory γ_{High} waves have their maximum peak (red star in Figure 6.a and Figure 6.b, respectively). This time series shows how the model generates a complex signal which closely resembles what is seen in the actual EEG and LFP data. The power spectrum of these time series is shown in Figure 9.

These results show that even with such a simple model of rhythm generation as the present one, a varied complex phenomenology can emerge in the system, including, e. g. the co-existence in time of different rhythms depending on certain parameter values. Analysis in depth of such complexity in a single work is difficult, so here we will focus on explaining the different behaviors observed in the region of dominant high γ oscillations, as we can connect this with currently discussions about the nature and meaning of HFO [17, 31, 47, 48, 52].

Comparing the variance in inhibitory activity shown in Figure 5.b and the region γ_{High} shown in Figure 6, the emergence of high frequency γ rhythms in excitatory groups appears to be related to the large variance observed in inhibitory activity in the high activity region (II.b). To help explore this apparent relation in more depth, we make scatter plots of the activity versus the maximum power spectrum density in the γ_{High} band for the high activity inhibitory region (II.b) shown in SI (Figure ??a).

We observed that there is no clear relation between excitatory firing activity and the emergence of high-frequency oscillations. However, we found that there is a minimum inhibitory firing rate that appears to be necessary to observe high-frequency oscillations in both neuron populations (Figures ??b and ??e); this does not mean that a higher inhibitory firing rate necessarily guarantees the emergence of these oscillations, but, as expected, shows that oscillations are related to interneurons (inhibitory activity).

Although there is no direct relationship between neuronal activity ρ and oscillations, as indicated previously, the temporal variance of activity does have a relationship with oscillations. We observe that the power density of the excitatory oscillations increases with the temporal variance of the inhibitory activity (Figures ??c in SI). There is also a relationship between the time variance of excitatory activity and inhibitory oscillations. However, such a relation is not as clear as in the inverse situation, since we observe that there is a region of parameter space where a high power level inhibitory γ_{High} band is observed, even with a low variance of excitatory activity (Figure ??f in SI). Therefore, only looking at the variance of the temporal activity is not enough to understand the emergence of these rhythms. A detailed discussion of these findings is presented in the SI.

Our analysis clearly illustrates that the emergence of high rhythms γ is not just a consequence of the high firing rate (see section 3 of SI), although the time variance of activity in one population appears to be related to the emergence of rhythms in the other. However, we find some exceptions, which show that this relation is not general. In conclusion, in the present model, despite its simplicity, the rhythms

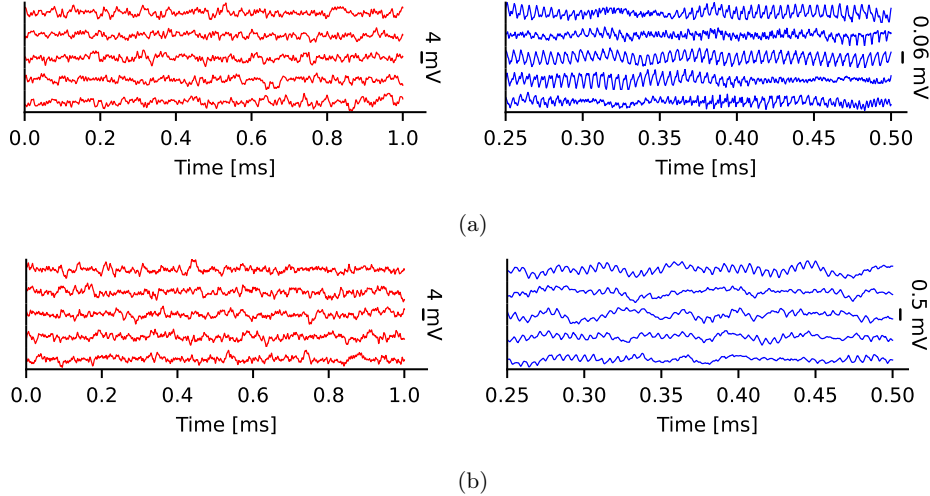


Figure 8: **Emergence of high γ in average membrane potential.** (a) High γ rhythms in excitatory (red) and inhibitory (blue) neuron groups at the point of maximum PSD in the high γ band (red star in Figure 6.a). The amplitudes of the inhibition oscillations are really small, and therefore, we do not consider it as relevant rhythms. (b) Coexistence of excitatory and inhibitory rhythms in the high γ band at the point (μ, τ_{rec}) of maximum PSD in the inhibitory population (red star in Figure 6.b). Here, the amplitude of inhibitory oscillations is 10 times larger than in (a), therefore, not negligible.

emerge as a complex interplay between excitatory and inhibitory populations. Global variables such as average neuronal activity (the typical mean-field observable used in the statistical mechanics approach) are not enough to explain this complexity.

In the next section, we will complement the study of the emergence of high-frequency oscillations using an information dynamics approach. We show that inhibitory γ_{High} emerge in regimes with low mutual information in inhibitory populations, indicating more randomness in the dynamics, while the region where excitatory γ_{High} waves are dominant maintains high mutual information in inhibitory population, with high redundancy in inhibitory group and high differentiation in excitatory group. This informational approach then shows new insights into the emergence of γ_{High} rhythms.

3.3 Information dynamics in the high γ oscillations regimes.

Now, we will focus on understanding the relation between the emergence of high γ rhythms and the complex information dynamics in the high EI activity phase. As a first step, we compute the time-delayed mutual information (TDMI) in each group, across the parameter space, in the region of interest. The results are shown in Figure 10, where the solid and dashed black curves indicate the region where excitatory and inhibitory γ_{High} dominate, respectively. We can see that TDMI in the excitatory neuron group does not show any relationship to the regions where excitatory γ_{High} emerges. However, it is possible to see that the region where inhibitory γ_{High} waves dominates matches precisely a region of low TDMI in the inhibitory population (blue region enclosed by black dashed line at the bottom of Figure 10.b). Other regions of low TDMI are also seen, but outside the region of high excitatory activity (II.b), which are related to lower activity in general and cannot be compared directly with the II.b phase.

Lower TDMI means that the knowledge of a past state gives us less information about the future state and viceversa, making the system less predictable or more random. On the other hand, finding a clearly lower TDMI region that matches the dominant inhibitory γ_{High} region means that, from an informational perspective, these waves are fundamentally different from the lower frequency excitatory γ_{High} . These results suggest that in our model, higher frequency HFOs are related to inhibitory oscillations, which are more random and, therefore, less functional. We will further explore these results by looking at the different information measures related to excitatory and inhibitory γ_{High} waves.

In the supplementary information document, we present complete information measures $(\Phi^R, \mathcal{U}, \mathcal{R})$ in the excitatory and inhibitory groups in Figure ?? and ??I. All points were measured in the high activity region (II.b), where γ_{High} rhythms emerge.

Excitatory γ_{High} rhythms appear to be related to higher differentiated information (Figure 11.c) and

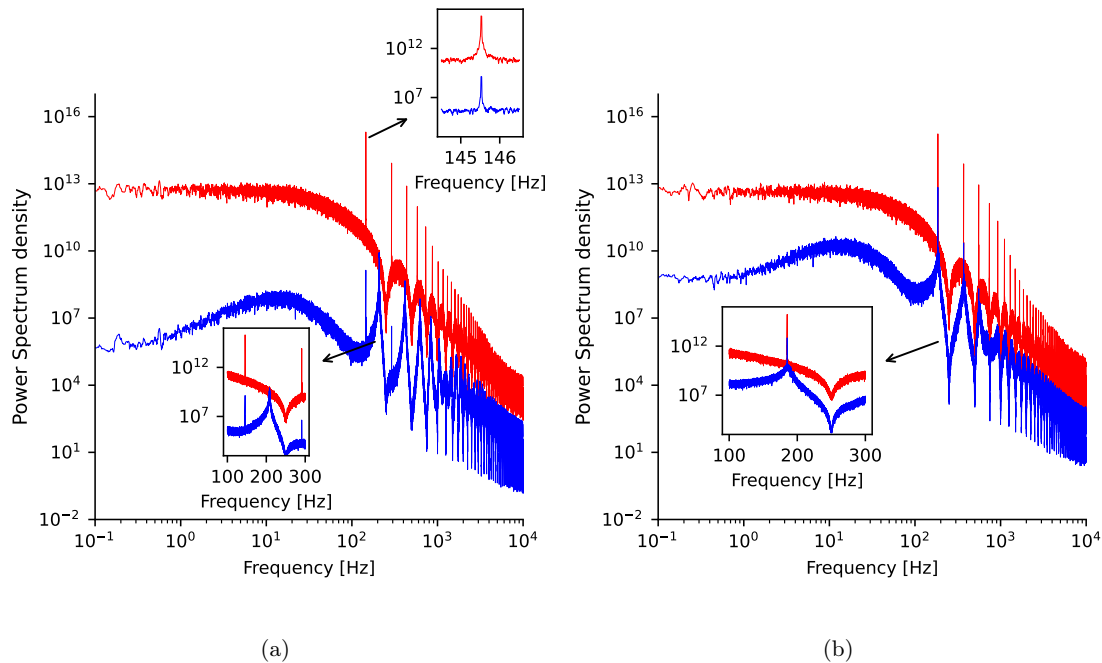


Figure 9: **Power spectrum density (PSD) of average membrane potential time serie.** (a) PSD of excitatory (red) and inhibitory (blue) neuron groups at the point of maximum PSD in the excitatory high γ band (red star in Figure 6.a). The figure depicts dominant oscillation frequency of the excitatory group around 145.5 Hz, while the inhibitory group shows low power oscillations at 200 Hz, which corresponds to the low amplitude inhibitory oscillations shown in Figure 8.a. A smaller peak of inhibitory oscillations is observed at 145.5Hz, seemingly induced by excitatory oscillations at the same frequency. (b) PSD of excitatory (red) and inhibitory (blue) neuron groups at the point of maximum PSD in the inhibitory high γ band (red star in Figure 6.b). Where excitatory and inhibitory oscillations coexist, both populations have a high power peak at the same frequency, close to 190 Hz. This frequency synchronization appears to be responsible for the increase in inhibitory oscillation amplitude shown in Figure 8. b, where the amplitudes are almost 10 times larger than in the 8.a.

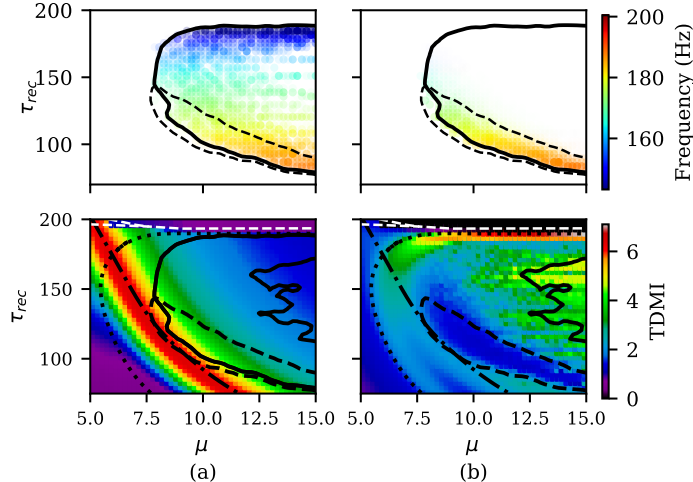


Figure 10: **Time-delayed mutual information and the emergence of high γ rhythms.** (Top) Peak frequency of oscillations where color opacity is directly proportional to the power spectrum density. (bottom) Time-delayed mutual information in (a) excitatory and (b) inhibitory neuron group. The solid black line indicates the region where high excitatory oscillations γ emerge (see Figure 6.a). The dashed black line indicates the region where high inhibitory oscillations γ of PSD $> 1 \times 10^9$ coexist with excitatory oscillations with PSD $> 1 \times 10^{11}$ (see Figure 6.b). (b,bottom) There is a clear relationship between lower mutual information and high inhibitory γ oscillations. Lower mutual information indicates that the system is less predictable, which means knowing past states gives us less information about the future of the system and vice versa. Dotted and dashed-dotted black lines indicate the maximum variance line of the inhibitory and excitatory neuron states X , respectively.

lower redundancy in the excitatory population (Figure ??c); while at the same time they are related to higher redundancy in inhibitory neurons (Figure 11.c). High redundancy indicates greater robustness to failures; while high differentiation indicates specialization, which means that each partitions is carrying different information and, therefore, are doing different operations. Together, these results indicate that, in this simple model, the dynamical regime in which excitatory γ_{High} oscillations dominate is more capable of robust specialized computational tasks. Note that this important conclusion can only be obtained using the current information dynamics framework.

In the region of high inhibitory redundancy and excitatory differentiation, dominant oscillations have a frequency of around 145 Hz. This frequency value is consistent with γ frequency interval often related to information processing in neuronal circuits [17]. Even when the specific cognitive function or mechanisms of these oscillations are still debated [23], the information dynamics properties observed in our study (higher excitatory differentiation combined with higher interneuron redundancy) seems to be adequate for a system capable of robust parallel information processing, as occurs in actual brains.

Higher frequencies ($> 250\text{Hz}$) are more often associated with pathological brain activity [39, 48], with exceptions. In our model, the γ_{High} frequencies which shows less functional information dynamics are of the order of 190Hz, closer to the limits usually associated with physiological high-frequency oscillations. Therefore, this result seems to be somehow compatible with the common notions related to HFOs, i.e. higher frequencies are more often related to pathological states, or in our case, to more random, less predictable interneurons dynamics.

Our results are especially intriguing because the system we are studying here is a priori too simple and not particularly designed (fine-tuned) to capture any specific properties of actual biological neuronal networks. Even more intriguing is the fact that the region where excitatory and inhibitory γ_{High} oscillations coexist and have the same frequency - almost 200 Hz - is also the region of phase II.b where mutual information is minimal (Figure 10 and Figure 12). This suggests that this “synchronization” of excitatory and inhibitory population frequency is related to a disruption in information flow in the inhibitory population, making the dynamics of this population more unpredictable or random.

With respect to integrated information in both excitatory and inhibitory groups, we found that points of maximum excitatory γ_{High} power show less integrated information (Fig.12.a), but this relationship is

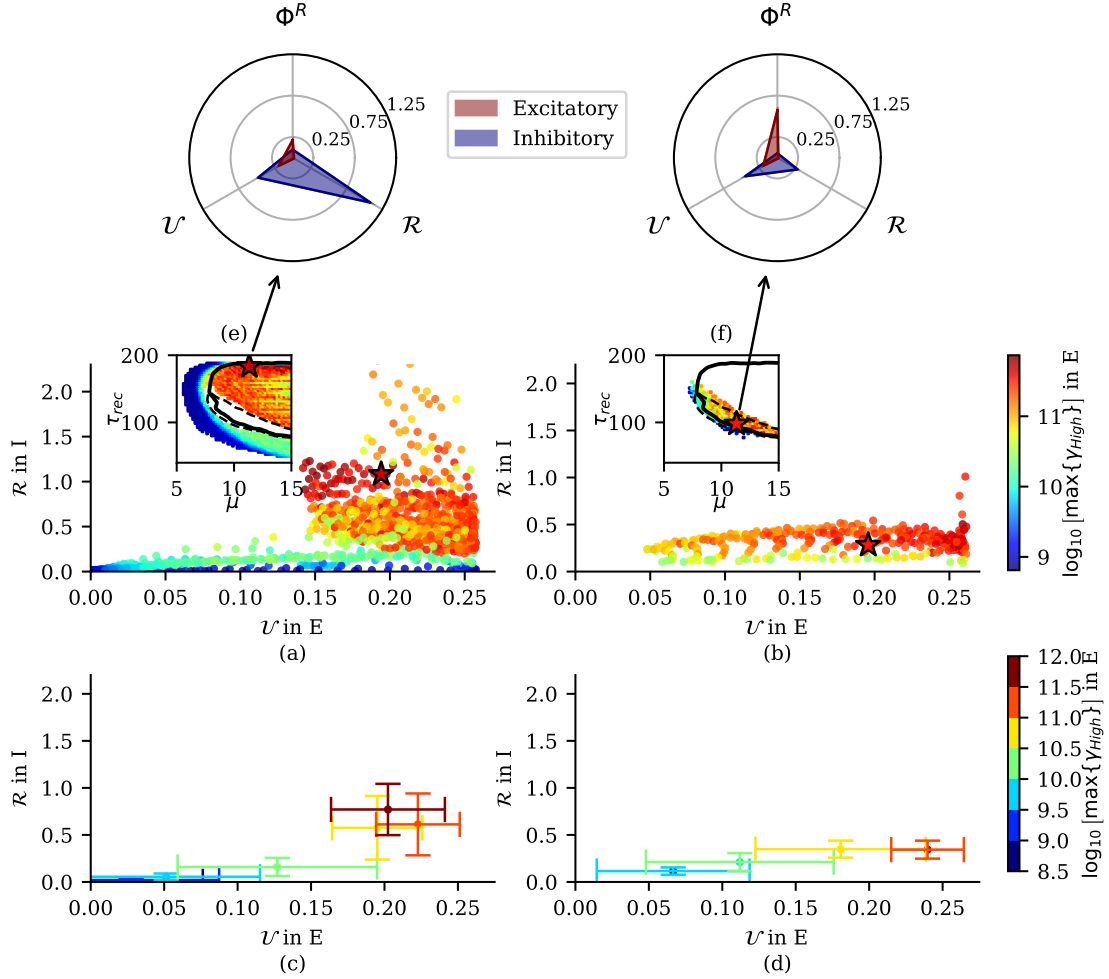


Figure 11: **Emergence of γ_{High} rhythms in E groups and the information dynamics of the system.** The colors indicate the level of maximum power density in the γ_{High} band. The data points in (a) correspond to points of high activity of the inhibitory population (region II.b) where there is no inhibitory high γ oscillation ($PSD < 10^9$) as shown in the inset (e) of the figure. The scatter plot of differentiated (\mathcal{U}) and redundant (\mathcal{R}) information in the excitatory and inhibitory groups, respectively, shows that the highest intensity of excitatory γ_{High} oscillations also have the highest \mathcal{U} and \mathcal{R} observed in the data. (b) The points were both excitatory and inhibitory, and high γ oscillations coexist, showing less redundancy information in the inhibitory population. (c and d) By grouping the data into PSD intervals, we compute the mean and standard deviation of the information measure values. In (c) it is clear that higher \mathcal{U} and \mathcal{R} are associated with dominant high γ oscillations ($PSD > 10^{10}$). The dynamic information diagram for two representative points of both regimes is also shown. The red star indicates the selected point. Both points have the same noise level μ and high amplitude γ_{High} in the excitatory population. The star color indicates its maximum power spectrum in the γ_{High} band following the color-bar.

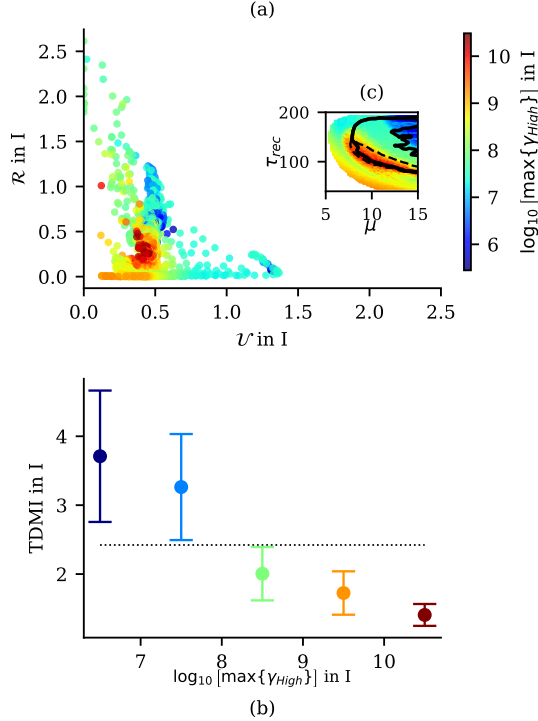


Figure 12: **Emergence of γ_{High} rhythms in I groups and information dynamics.** Colors indicate the level of maximum power density in the γ_{High} band. The data points in (a) correspond to points of high activity of the inhibitory population (region II.b) as shown in the inset (c) of the figure. The scatter plot of differentiated (\mathcal{U}) and redundant (\mathcal{R}) information in inhibitory groups, respectively, shows that the points of highest intensity of inhibitory high γ oscillations have the lowest \mathcal{U} and \mathcal{R} observed in the data. These points are those where excitatory and inhibitory oscillations coexist (Figure 11. f). (b) By grouping data in power spectrum density intervals and computing the mean and standard deviation of time-delayed mutual information (TDMI), we observe a clear inverse relation between inhibitory oscillations amplitude and mutual information. The black dashed lines in (b) are the average TDMI of all data.

not clear as some exceptions are observed. On the other hand, while inhibitory γ_{High} does not appear to be related to the level of integrated information in the excitatory group, it shows a clear relation with the lower values of integrated information in the inhibitory group (Fig.12.b). The clear relation between high frequency oscillations in the inhibitory group and lower values of integrated information agrees with the observation of a lower TDMI, as integrated information is part of the TDMI measure. This behavior supports our interpretation that inhibitory γ_H waves in our model emerge in more random dynamical regimes where interneurons will be less capable of sustaining higher information processing.

3.4 Limitations of our analysis from experimental point of view

The results observed from the information dynamics analysis in our system suggest the following hypothesis to be tested in experiments: Pathological HFOs, usually related to epileptic seizures, have a less rich information dynamics characterized by a decrease in mutual information between different parts of the neuronal network, while physiological HFOs will maintain high mutual information with high differentiation and redundancy.

To test this hypothesis in experiments, we have two paths: The first one is to obtain high spatial and temporal resolution data of neurons activity in regions where HFOs emerge, in both pathological and physiological cases, and apply the same analysis done here in the data. For our model analysis, large time series (2×10^5 time bins) of a small group of neurons spike trains were used. Data with such details will not always be accessible from an experimental point of view.

The second path, more accessible, is to apply the information dynamics analysis directly over meso-

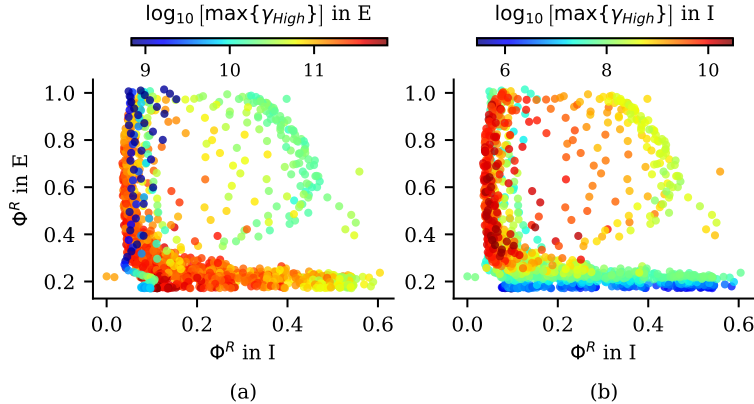


Figure 13: **Emergence of γ_{High} rhythms and the integrated information.** The data points correspond to the high activity of the inhibitory population (region II.b) as in Figures 12 and 13. The scatter plot of these points shows the values of the integrated information (Φ^R) in the excitatory and inhibitory groups at each point. The colors indicate the maximum power density level in the (a) excitatory and (b) inhibitory γ_{High} band. Points with high power γ_{High} appear to concentrate in regions of lower integrated information in inhibitory groups.

scopic/macrosopic variables such as LFP, EEG or MEG, given a sufficient spatial resolution of the brain region of interest. The information dynamics analysis of our model follows the first path, but the second path could also be performed directly over the average membrane potential of our neuron groups. Φ -ID have not limitations with respect to the type of variable used and it can and was applied to both discrete and continuous variables, including EEG data. However, when dealing with continuous data, probability distributions and mutual information estimation are trickier and introduce more arbitrariness with respect to estimator methods, which require high level of expertise to justify the methods applied. Commonly used methods based on k-nearest-neighbor (kNN) methods introduce bias and errors that should be carefully considered [24, 49].

Despite the fact that in the last decade new techniques have been continually developed to address the limitations and bias of continuous-variable mutual information estimation methods, we consider the development of discretization methods for continuous variables, such as ordered patterns [7], a more efficient way of dealing with the problems cited [38, 69]. In this case, information dynamics analysis could be applied to discrete variables using simple discrete probability estimators, such as counting bins, which are less problematic in discrete data. This and other questions related to continuous variables in our model will be addressed in future work.

4 Conclusions

In this work we have explored an EEG neuronal network model from a dynamical and informational point of view which allowed us to expand our understanding about the complex behavior of this relatively simple system. The dynamical approach revealed different phase transitions, most of which were already described in the previous literature of this model [20][51]. However, in the present work we also identified what appears to be a low-activity intermediate phase (LAI phase) for both excitatory and inhibitory populations with a transition to a high-activity phase, which was not previously reported. Also, we have studied here the main features of such phases and the complex interplay between E and I neuron populations to induce such phases.

More precisely, through spectral analysis of the average membrane potential of groups of excitatory and inhibitory neurons, we identified the regions in this space where the different waves (δ , θ , α , β and γ) emerge and are dominant. More important, we find that HFO rhythms emerge in a specific region of the phase diagram of the EEG model characterized by external noise level $\mu > 7$ and synaptic resource recovery time $100 < \tau_{rec} < 200$, which were not explored in previous literature. Therefore we focused on characterizing the region of phase space where HFOs emerge.

Interesting, the high frequency waves show a complex pattern across the high activity phase space and matches with high fluctuations in the inhibitory population activity. We also have shown that HFOs

observed in excitatory and inhibitory populations are not the same across the phase space. The region where both oscillations have the same frequency depicts an increase in inhibitory wave amplitudes and an increase in excitatory oscillation frequency. The region where the frequencies do not match illustrates a much lower amplitude of inhibitory waves maintaining high frequencies, while excitatory HFOs dominate but with lower frequencies. This result suggests two different HFO regimes, one of excitatory / inhibitory oscillations with same dominant frequency (≈ 200 Hz) and the other with excitatory/inhibitory oscillations with different frequencies where excitatory oscillations are dominant and have lower frequency (≈ 145 Hz).

To better characterize the apparent different HFO regimes, we explore them from the perspective of informational dynamics of neuronal activity applying the integrated information decomposition (Φ -ID) framework. Using the different information atoms obtained from Φ -ID analysis, we defined information measures to describe the three main modes of information dynamics, which are redundant information (information shared by many parts of the system), differentiated information (information unique to different parts of the system), and integrated information (information that emerges synergistically).

The present informational analysis allowed us to clearly identify the differences between the two found HFO regimes. In the first region, where the lower-frequency excitatory γ_{High} waves dominate, we observed a higher excitatory information differentiation and higher inhibitory redundancy. The second region, where excitatory/inhibitory oscillations synchronize and inhibitory γ_{High} waves dominate, has lower mutual information as a whole, indicating a more random evolution of the system states. Both regions have clearly different information dynamical properties; while the first seems suitable for information processing, and therefore we can relate in some sense with physiological or functional regimes, the second one is less predictable, less robust with poor informational properties, and therefore it can be associated to a pathological regime.

Although our model is simple, it could be very suitable to investigate some functional properties of actual neural systems, such as cortical dynamics. This is mainly due to the rich repertoire of emerging behaviors, both from the dynamical and from the information dynamics perspective, which allow us to obtain possible functional insights about the different observed rhythms. The information dynamics measures used to describe local dynamics in combination with the more mesoscopic spectral measure of neuron membrane potential give us a surprisingly coherent picture of possible fundamental differences between physiological and pathological conditions in HFOs, which could be further explored both from computational and experimental perspectives.

Differentiating HFOs from experimental data is important in the clinical diagnoses of epileptic seizures and the identification of epileptogenic regions. In the case of our simple computational model, it seems that an informational dynamical approach may be the right way to identify physiological and pathological HFOs. Therefore, in the future we will explore the hypothesis derived from the present study in experimental data related to physiological and pathological HFOs and epileptic seizures.

5 Acknowledgements

G.M. would like to thank the *Programa Nacional de Becas de Postgrados en el Exterior "Don Carlos Antonio López"(BECAL)-Paraguay* for the financial support to his doctoral studies in the Physics and Mathematics Program of the University of Granada. J.J.T. acknowledges financial support from the Consejería de Transformación Económica, Industria, Conocimiento y Universidades, Spain, Junta de Andalucía, Spain and European Regional Development Funds, Ref. P20_00173. This work is also part of the Project of I+D+i, Spain Ref. PID2020 113681GBI00, financed by MICIN/AEI/10.13039/501100011033 and FEDER, Spain "Away to make Europe". The authors thank Pedro A. M. Mediano for fruitful discussions and comments.

References

- [1] The emergence of integrated information, complexity, and 'consciousness' at criticality. *Entropy*, 22: 339, 3 2020. ISSN 1099-4300. doi:10.3390/e22030339.
- [2] An implementation of integrated information theory in resting-state fmri. *Communications Biology*, 6:692, 7 2023. ISSN 2399-3642. doi:10.1038/s42003-023-05063-y.
- [3] Miguel Aguilera. Scaling behaviour and critical phase transitions in integrated information theory. *Entropy*, 21, 12 2019. ISSN 10994300. doi:10.3390/e21121198.

- [4] Miguel Aguilera and Ezequiel A. Di Paolo. Critical integration in neural and cognitive systems: Beyond power-law scaling as the hallmark of soft assembly. *Neuroscience & Biobehavioral Reviews*, 123:230–237, 4 2021. ISSN 01497634. doi:10.1016/j.neubiorev.2021.01.009.
- [5] Rafeed Alkawadri and Lawrence J. Hirsch. Fast, very fast, ultrafast, and even faster: How high frequency should we be recording on intracranial eeg? *Epilepsy Currents*, 18:217–219, 7 2018. ISSN 1535-7597. doi:10.5698/1535-7597.18.4.217. URL <http://journals.sagepub.com/doi/10.5698/1535-7597.18.4.217>.
- [6] David Balduzzi and Giulio Tononi. Integrated information in discrete dynamical systems: Motivation and theoretical framework. *PLoS Computational Biology*, 4, 2008. ISSN 15537358. doi:10.1371/journal.pcbi.1000091.
- [7] Christoph Bandt. Order patterns, their variation and change points in financial time series and brownian motion. *Statistical Papers*, 61:1565–1588, 8 2020. ISSN 0932-5026. doi:10.1007/s00362-020-01171-7.
- [8] Adam B. Barrett. Exploration of synergistic and redundant information sharing in static and dynamical gaussian systems. *Physical Review E - Statistical, Nonlinear, and Soft Matter Physics*, 91, 5 2015. ISSN 15502376. doi:10.1103/PhysRevE.91.052802.
- [9] Milan Brázdil, Martin Pail, Josef Halámek, Filip Plešinger, Jan Cimbálník, Robert Roman, Petr Klimeš, Pavel Daniel, Jan Chrastina, Eva Brichtová, Ivan Rektor, Gregory A. Worrell, and Pavel Jurák. Very high-frequency oscillations: Novel biomarkers of the epileptogenic zone. *Annals of Neurology*, 82:299–310, 8 2017. ISSN 03645134. doi:10.1002/ana.25006.
- [10] Victor Buendía, Pablo Villegas, Serena di Santo, Alessandro Vezzani, Raffaella Burioni, and Miguel A. Muñoz. Jensen’s force and the statistical mechanics of cortical asynchronous states. *Sci. Rep.*, 9:15183, 10 2019. ISSN 2045-2322. doi:10.1038/s41598-019-51520-2.
- [11] György Buzsáki. Rhythms of the brain, 10 2006.
- [12] Jonathan Cannon, Michelle M. McCarthy, Shane Lee, Jung Lee, Christoph Börgers, Miles A. Whittington, and Nancy Kopell. Neurosystems: brain rhythms and cognitive processing. *European Journal of Neuroscience*, 39(5):705–719, 2014. doi:https://doi.org/10.1111/ejn.12453. <https://onlinelibrary.wiley.com/doi/pdf/10.1111/ejn.12453>. URL <https://onlinelibrary.wiley.com/doi/abs/10.1111/ejn.12453>.
- [13] Thomas M. Cover and Joy A. Thomas. Elements of information theory 2nd edition (wiley series in telecommunications and signal processing). Hardcover, July 2006.
- [14] F. H. Lopes da Silva, A. Hoeks, H. Smits, and L. H. Zetterberg. Model of brain rhythmic activity. *Kybernetik*, 15:27–37, 3 1974. ISSN 0023-5946. doi:10.1007/BF00270757.
- [15] Andreas K Engel and Pascal Fries. Beta-band oscillations — signalling the status quo? *Current Opinion in Neurobiology*, 20:156–165, 4 2010. ISSN 09594388. doi:10.1016/j.conb.2010.02.015.
- [16] F.R. Farina, D.D. Emek-Savaş, L. Rueda-Delgado, R. Boyle, H. Kiiski, G. Yener, and R. Whelan. A comparison of resting state eeg and structural mri for classifying alzheimer’s disease and mild cognitive impairment. *NeuroImage*, 215:116795, 2020. ISSN 1053-8119. doi:https://doi.org/10.1016/j.neuroimage.2020.116795. URL <https://www.sciencedirect.com/science/article/pii/S1053811920302822>.
- [17] Antonio Fernandez-Ruiz, Anton Sirota, Vítor Lopes dos Santos, and David Dupret. Over and above frequency: Gamma oscillations as units of neural circuit operations. *Neuron*, 111:936–953, 4 2023. ISSN 08966273. doi:10.1016/j.neuron.2023.02.026. URL <https://linkinghub.elsevier.com/retrieve/pii/S0896627323001307>.
- [18] Gord Fishell and Adam Kepecs. Interneuron types as attractors and controllers. *Annual Review of Neuroscience*, 43:1–30, 7 2020. ISSN 0147-006X. doi:10.1146/annurev-neuro-070918-050421.
- [19] Birgit Frauscher, Fabrice Bartolomei, Katsuhiko Kobayashi, Jan Cimbálník, Maryse A. van ‘t Klooster, Stefan Rampp, Hiroshi Otsubo, Yvonne Höller, Joyce Y. Wu, Eishi Asano, Jerome Engel, Philippe Kahane, Julia Jacobs, and Jean Gotman. High-frequency oscillations: The state of clinical research. *Epilepsia*, 58:1316–1329, 8 2017. ISSN 00139580. doi:10.1111/epi.13829.

- [20] Javier A. Galadí, Joaquín J. Torres, and J. Marro. Emergence and interpretation of oscillatory behaviour similar to brain waves and rhythms. *Communications in Nonlinear Science and Numerical Simulation*, 83:105093, 2020. ISSN 1007-5704. doi:<https://doi.org/10.1016/j.cnsns.2019.105093>. URL <https://www.sciencedirect.com/science/article/pii/S1007570419304125>.
- [21] Lukas A W Gemein, Robin T Schirrmester, Patryk Chrabąszcz, Daniel Wilson, Joshka Boedecker, Andreas Schulze-Bonhage, Frank Hutter, and Tonio Ball. Machine-learning-based diagnostics of EEG pathology. *Neuroimage*, 220:117021, June 2020.
- [22] Reza Ghorbanchian, Juan G. Restrepo, Joaquín J. Torres, and Ginestra Bianconi. Higher-order simplicial synchronization of coupled topological signals. *Communications Physics*, 4(1):120, Jun 2021. ISSN 2399-3650. doi:[10.1038/s42005-021-00605-4](https://doi.org/10.1038/s42005-021-00605-4). URL <https://doi.org/10.1038/s42005-021-00605-4>.
- [23] Chuanliang Han, Robert Shapley, and Dajun Xing. Gamma rhythms in the visual cortex: functions and mechanisms. *Cognitive Neurodynamics*, 16:745–756, 8 2022. ISSN 18714099. doi:[10.1007/s11571-021-09767-x](https://doi.org/10.1007/s11571-021-09767-x).
- [24] Caroline M. Holmes and Ilya Nemenman. Estimation of mutual information for real-valued data with error bars and controlled bias. *Physical Review E*, 100:022404, 8 2019. ISSN 2470-0045. doi:[10.1103/PhysRevE.100.022404](https://doi.org/10.1103/PhysRevE.100.022404).
- [25] Shinya Ito, Michael E. Hansen, Randy Heiland, Andrew Lumsdaine, Alan M. Litke, and John M. Beggs. Extending transfer entropy improves identification of effective connectivity in a spiking cortical network model. *PLoS ONE*, 6:e27431, 11 2011. ISSN 1932-6203. doi:[10.1371/journal.pone.0027431](https://doi.org/10.1371/journal.pone.0027431).
- [26] Skyler L. Jackman and Wade G. Regehr. The mechanisms and functions of synaptic facilitation. *Neuron*, 94:447–464, 5 2017. ISSN 08966273. doi:[10.1016/j.neuron.2017.02.047](https://doi.org/10.1016/j.neuron.2017.02.047).
- [27] Henrik Jeldtoft Jensen. *Self-Organized Criticality: Emergent Complex Behavior in Physical and Biological Systems*. Cambridge Lecture Notes in Physics. Cambridge University Press, 1998. doi:[10.1017/CB09780511622717](https://doi.org/10.1017/CB09780511622717).
- [28] Joram Keijser and Henning Sprekeler. Optimizing interneuron circuits for compartment-specific feedback inhibition. *PLOS Computational Biology*, 18:e1009933, 4 2022. ISSN 1553-7358. doi:[10.1371/journal.pcbi.1009933](https://doi.org/10.1371/journal.pcbi.1009933).
- [29] Kim and Lee. Criticality as a determinant of integrated information ϕ in human brain networks. *Entropy*, 21:981, 10 2019. ISSN 1099-4300. doi:[10.3390/e21100981](https://doi.org/10.3390/e21100981).
- [30] Juri D. Kropotov. *Beta and Gamma Rhythms*, pages 107–119. Elsevier, 2016. doi:[10.1016/B978-0-12-410513-3.00009-7](https://doi.org/10.1016/B978-0-12-410513-3.00009-7).
- [31] Michal T. Kucewicz, Jan Cimbalk, Joseph Y. Matsumoto, Benjamin H. Brinkmann, Mark R. Bower, Vincent Vasoli, Vlastimil Sulc, Fred Meyer, W. R. Marsh, S. M. Stead, and Gregory A. Worrell. High frequency oscillations are associated with cognitive processing in human recognition memory. *Brain*, 137:2231–2244, 2014. ISSN 14602156. doi:[10.1093/brain/awu149](https://doi.org/10.1093/brain/awu149).
- [32] Joseph T. Lizier. The local information dynamics of distributed computation in complex systems, 2013. URL <https://link.springer.com/10.1007/978-3-642-32952-4>.
- [33] Andrea I. Luppi, Pedro A.M. Mediano, Fernando E. Rosas, David J. Harrison, Robin L. Carhart-Harris, Daniel Bor, and Emmanuel A. Stamatakis. What it is like to be a bit: an integrated information decomposition account of emergent mental phenomena. *Neuroscience of Consciousness*, 2021, 2021. ISSN 20572107. doi:[10.1093/nc/niab027](https://doi.org/10.1093/nc/niab027).
- [34] Andrea I. Luppi, Pedro A. M. Mediano, Fernando E. Rosas, Negin Holland, Tim D. Fryer, John T. O’Brien, James B. Rowe, David K. Menon, Daniel Bor, and Emmanuel A. Stamatakis. A synergistic core for human brain evolution and cognition. *Nature Neuroscience*, 25:771–782, 6 2022. ISSN 1097-6256. doi:[10.1038/s41593-022-01070-0](https://doi.org/10.1038/s41593-022-01070-0).

- [35] Víctor J López-Madrona, Elena Pérez-Montoyo, Efrén Álvarez Salvado, David Moratal, Oscar Herreras, Ernesto Pereda, Claudio R Mirasso, and Santiago Canals. Different theta frameworks coexist in the rat hippocampus and are coordinated during memory-guided and novelty tasks. *eLife*, 9:e57313, jul 2020. ISSN 2050-084X. doi:10.7554/eLife.57313. URL <https://doi.org/10.7554/eLife.57313>.
- [36] Gianmaria Maccaferri and Jean-Claude Lacaille. Interneuron diversity series: Hippocampal interneuron classifications – making things as simple as possible, not simpler. *Trends in Neurosciences*, 26:564–571, 10 2003. ISSN 01662236. doi:10.1016/j.tins.2003.08.002.
- [37] Joaquin Marro and Joaquin J. Torres. Phase Transitions in Grey Matter: Brain Architecture and Mind Dynamics. URL <https://doi.org/10.1063/9780735421769>.
- [38] Diego M. Mateos, Jaime Gómez-Ramírez, and Osvaldo A. Rosso. Using time causal quantifiers to characterize sleep stages. *Chaos, Solitons & Fractals*, 146:110798, 5 2021. ISSN 09600779. doi:10.1016/j.chaos.2021.110798.
- [39] Andrew Matsumoto, Benjamin H. Brinkmann, S. Matthew Stead, Joseph Matsumoto, Michal T. Kucewicz, W. Richard Marsh, Frederic Meyer, and Gregory Worrell. Pathological and physiological high-frequency oscillations in focal human epilepsy. *Journal of Neurophysiology*, 110:1958–1964, 10 2013. ISSN 0022-3077. doi:10.1152/jn.00341.2013.
- [40] Pedro A. M. Mediano, Fernando E. Rosas, Andrea I Luppi, Robin L. Carhart-Harris, Daniel Bor, Anil K. Seth, and Adam B. Barrett. Towards an extended taxonomy of information dynamics via integrated information decomposition. 9 2021.
- [41] Pedro A. M. Mediano, Fernando E. Rosas, Juan Carlos Farah, Murray Shanahan, Daniel Bor, and Adam B. Barrett. Integrated information as a common signature of dynamical and information-processing complexity. *Chaos: An Interdisciplinary Journal of Nonlinear Science*, 32:013115, 1 2022. ISSN 1054-1500. doi:10.1063/5.0063384.
- [42] J. F. Mejias, B. Hernandez-Gomez, and J. J. Torres. Short-term synaptic facilitation improves information retrieval in noisy neural networks. *Europhysics Letters*, 97(4):48008, feb 2012. doi:10.1209/0295-5075/97/48008. URL <https://dx.doi.org/10.1209/0295-5075/97/48008>.
- [43] Gustavo Menesse and Osame Kinouchi. Less is different: Why sparse networks with inhibition differ from complete graphs. *Physical Review E*, 108:024315, 8 2023. ISSN 2470-0045. doi:10.1103/PhysRevE.108.024315.
- [44] Ana P. Millán, J. J. Torres, S. Johnson, and J. Marro. Concurrence of form and function in developing networks and its role in synaptic pruning. *Nature Communications*, 9(1):2236, Jun 2018. ISSN 2041-1723. doi:10.1038/s41467-018-04537-6. URL <https://doi.org/10.1038/s41467-018-04537-6>.
- [45] Ana P. Millán, Joaquín J. Torres, and Ginestra Bianconi. Explosive higher-order kuramoto dynamics on simplicial complexes. *Phys. Rev. Lett.*, 124:218301, May 2020. doi:10.1103/PhysRevLett.124.218301. URL <https://link.aps.org/doi/10.1103/PhysRevLett.124.218301>.
- [46] Anne H. Mooij, Geertjan J.M. Huiskamp, Emmeke Aarts, Cyrille H. Ferrier, Kees P.J. Braun, and Maeike Zijlmans. Accurate differentiation between physiological and pathological ripples recorded with scalp-eeg. *Clinical Neurophysiology*, 143:172–181, 11 2022. ISSN 13882457. doi:10.1016/j.clinph.2022.08.014.
- [47] Lotte Noorlag, Nicole E.C. van Klink, Katsuhiko Kobayashi, Jean Gotman, Kees P.J. Braun, and Maeike Zijlmans. High-frequency oscillations in scalp eeg: A systematic review of methodological choices and clinical findings. *Clinical Neurophysiology*, 137:46–58, 5 2022. ISSN 18728952. doi:10.1016/j.clinph.2021.12.017.
- [48] Chae Jung Park and Seung Bong Hong. High frequency oscillations in epilepsy: Detection methods and considerations in clinical application. *Journal of Epilepsy Research*, 9:1–13, 1 2019. ISSN 2233-6249. doi:10.14581/jer.19001. URL <http://www.j-epilepsy.org/journal/view.php?doi=10.14581/jer.19001>.

- [49] Fernando Pérez-Cruz. Estimation of information theoretic measures for continuous random variables. In D. Koller, D. Schuurmans, Y. Bengio, and L. Bottou, editors, *Advances in Neural Information Processing Systems*, volume 21. Curran Associates, Inc., 2008. URL https://proceedings.neurips.cc/paper_files/paper/2008/file/ccb0989662211f61edae2e26d58ea92f-Paper.pdf.
- [50] Francesco Precenzano, Lucia Parisi, Valentina Lanzara, Luigi Vetri, Francesca Felicia Operto, Grazia Maria Giovanna Pastorino, Maria Ruberto, Giovanni Messina, Maria Cristina Risoleo, Claudia Santoro, Ilaria Bitetti, and Rosa Marotta. Electroencephalographic abnormalities in autism spectrum disorder: Characteristics and therapeutic implications. *Medicina (Kaunas)*, 56(9), August 2020.
- [51] Jorge Pretel, Joaquín J. Torres, and Joaquín Marro. Eegs disclose significant brain activity correlated with synaptic fickleness. *Biology*, 10(7), 2021. ISSN 2079-7737. doi:10.3390/biology10070647. URL <https://www.mdpi.com/2079-7737/10/7/647>.
- [52] Supratim Ray, Ernst Niebur, Steven S. Hsiao, Alon Sinai, and Nathan E. Crone. High-frequency gamma activity (80–150hz) is increased in human cortex during selective attention. *Clinical Neurophysiology*, 119:116–133, 1 2008. ISSN 13882457. doi:10.1016/j.clinph.2007.09.136. URL <https://linkinghub.elsevier.com/retrieve/pii/S1388245707005159>.
- [53] Fernando E. Rosas, Pedro A.M. Mediano, Borzoo Rassouli, and Adam B. Barrett. An operational information decomposition via synergistic disclosure. *Journal of Physics A: Mathematical and Theoretical*, 53, 12 2020. ISSN 17518121. doi:10.1088/1751-8121/abb723.
- [54] B.J. Ruijter, J. Hofmeijer, H.G.E. Meijer, and M.J.A.M. van Putten. Synaptic damage underlies eeg abnormalities in postanoxic encephalopathy: A computational study. *Clinical Neurophysiology*, 128(9):1682–1695, 2017. ISSN 1388-2457. doi:<https://doi.org/10.1016/j.clinph.2017.06.245>. URL <https://www.sciencedirect.com/science/article/pii/S1388245717304728>.
- [55] S J M Smith. Eeg in the diagnosis, classification, and management of patients with epilepsy. *Journal of Neurology, Neurosurgery & Psychiatry*, 76(suppl 2):ii2–ii7, 2005. ISSN 0022-3050. doi:10.1136/jnnp.2005.069245.
- [56] Nirit Sukenik, Oleg Vinogradov, Eyal Weinreb, Menahem Segal, Anna Levina, and Elisha Moses. Neuronal circuits overcome imbalance in excitation and inhibition by adjusting connection numbers. *Proceedings of the National Academy of Sciences*, 118(12):e2018459118, 2021. doi:10.1073/pnas.2018459118. <https://www.pnas.org/doi/pdf/10.1073/pnas.2018459118>. URL <https://www.pnas.org/doi/abs/10.1073/pnas.2018459118>.
- [57] Nicholas M. Timme, Najja J. Marshall, Nicholas Bennett, Monica Ripp, Edward Lautzenhiser, and John M. Beggs. Criticality maximizes complexity in neural tissue. *Frontiers in Physiology*, 7, 9 2016. ISSN 1664-042X. doi:10.3389/fphys.2016.00425.
- [58] J. J. Torres, J. M. Cortes, J. Marro, and H. J. Kappen. Competition between synaptic depression and facilitation in attractor neural networks. *Neural Computation*, 19(10):2739–2755, 10 2007. ISSN 0899-7667. doi:10.1162/neco.2007.19.10.2739. <https://direct.mit.edu/neco/article-pdf/19/10/2739/816974/neco.2007.19.10.2739.pdf>. URL <https://doi.org/10.1162/neco.2007.19.10.2739>.
- [59] J J Torres, J Marro, and J F Mejias. Can intrinsic noise induce various resonant peaks? *New Journal of Physics*, 13(5):053014, may 2011. doi:10.1088/1367-2630/13/5/053014. URL <https://dx.doi.org/10.1088/1367-2630/13/5/053014>.
- [60] J.J. Torres, M.A. Muñoz, J. Marro, and P.L. Garrido. Influence of topology on the performance of a neural network. *Neurocomputing*, 58-60:229–234, 2004. ISSN 0925-2312. doi:<https://doi.org/10.1016/j.neucom.2004.01.048>. URL <https://www.sciencedirect.com/science/article/pii/S092523120400044X>. Computational Neuroscience: Trends in Research 2004.
- [61] Joaquin J. Torres and Hilbert J. Kappen. Emerging phenomena in neural networks with dynamic synapses and their computational implications. *Frontiers in Computational Neuroscience*, 7, 2013. ISSN 1662-5188. doi:10.3389/fncom.2013.00030. URL <https://www.frontiersin.org/articles/10.3389/fncom.2013.00030>.

- [62] Joaquin J. Torres, Irene Elices, and J. Marro. Efficient transmission of subthreshold signals in complex networks of spiking neurons. *PLOS ONE*, 10:1–22, 03 2015. doi:10.1371/journal.pone.0121156. URL <https://doi.org/10.1371/journal.pone.0121156>.
- [63] Joaquín J Torres and Ginestra Bianconi. Simplicial complexes: higher-order spectral dimension and dynamics. *Journal of Physics: Complexity*, 1(1):015002, may 2020. doi:10.1088/2632-072X/ab82f5. URL <https://dx.doi.org/10.1088/2632-072X/ab82f5>.
- [64] Misha Tsodyks and Henry Markram. The neural code between neocortical pyramidal neurons depends on neurotransmitter release probability. *Proceedings of the National Academy of Sciences*, 94(2):719–723, 1997. doi:10.1073/pnas.94.2.719. <https://www.pnas.org/doi/pdf/10.1073/pnas.94.2.719>. URL <https://www.pnas.org/doi/abs/10.1073/pnas.94.2.719>.
- [65] Misha Tsodyks, Klaus Pawelzik, and Henry Markram. Neural Networks with Dynamic Synapses. *Neural Computation*, 10(4):821–835, 05 1998. ISSN 0899-7667. doi:10.1162/089976698300017502. <https://direct.mit.edu/neco/article-pdf/10/4/821/813807/089976698300017502.pdf>. URL <https://doi.org/10.1162/089976698300017502>.
- [66] Thomas F. Varley. Decomposing past and future: Integrated information decomposition based on shared probability mass exclusions. *PLOS ONE*, 18:e0282950, 3 2023. ISSN 1932-6203. doi:10.1371/journal.pone.0282950.
- [67] J J Wright. Simulation of EEG: dynamic changes in synaptic efficacy, cerebral rhythms, and dissipative and generative activity in cortex. *Biol Cybern*, 81(2):131–147, August 1999.
- [68] Kai Yang, Li Tong, Jun Shu, Ning Zhuang, Bin Yan, and Ying Zeng. High gamma band eeg closely related to emotion: Evidence from functional network. *Frontiers in Human Neuroscience*, 14, 3 2020. ISSN 16625161. doi:10.3389/fnhum.2020.00089.
- [69] Massimiliano Zanin and Felipe Olivares. Ordinal patterns-based methodologies for distinguishing chaos from noise in discrete time series. *Communications Physics*, 4:190, 8 2021. ISSN 2399-3650. doi:10.1038/s42005-021-00696-z.

Information dynamics efficiently discriminates high γ -rhythms in EEG brain waves Supplementary information

Gustavo Menesse^{1*} Joaquín J. Torres¹

¹Organization 1
{auth1, auth3}@org1.edu
²Organization 2
auth3@inst2.edu

1 Power spectrum density across phase diagram

Figure S1 shows the maxima in the power spectrum for each band in the parameter space (μ, τ_{rec}) . We can observe many interesting behaviors, such as modulations of β frequencies by δ frequency oscillations in the metastable region (between dashed white lines), but also the emergence of low frequency rhythms (δ, θ, α) , a region of high inhibitory activity, between the LAI-like phase transition of both populations (between dashed-dotted and dotted white lines).

Figures S2a and S2b show the average membrane potential of 5 groups of excitatory (a) and inhibitory (b) neurons at different points of the parameter space (μ, τ_{rec}) . An interesting observation is that high-frequency oscillations (γ_{High}) in excitatory neurons are less noisy than high-frequency oscillations in the inhibitory population, which is related to less mutual information values in the inhibitory population in the region where the inhibitory γ_{High} emerges.

The full power spectrum densities for different values of τ_{rec} fixing μ are shown in Figures S3a,S3b,S3c, and for different values of μ fixing τ_{rec} in Figures S4a,S4b,S4c. In these figures, we apply a moving average for the power spectrum between the frequencies 0 and 100 Hz. This helps to visualize the different curves, but by doing so we modify the power intensities, and this is the reason why the values in these plots do not match the maximum values shown in the latest figures.

*Author One was supported by Grant XXX

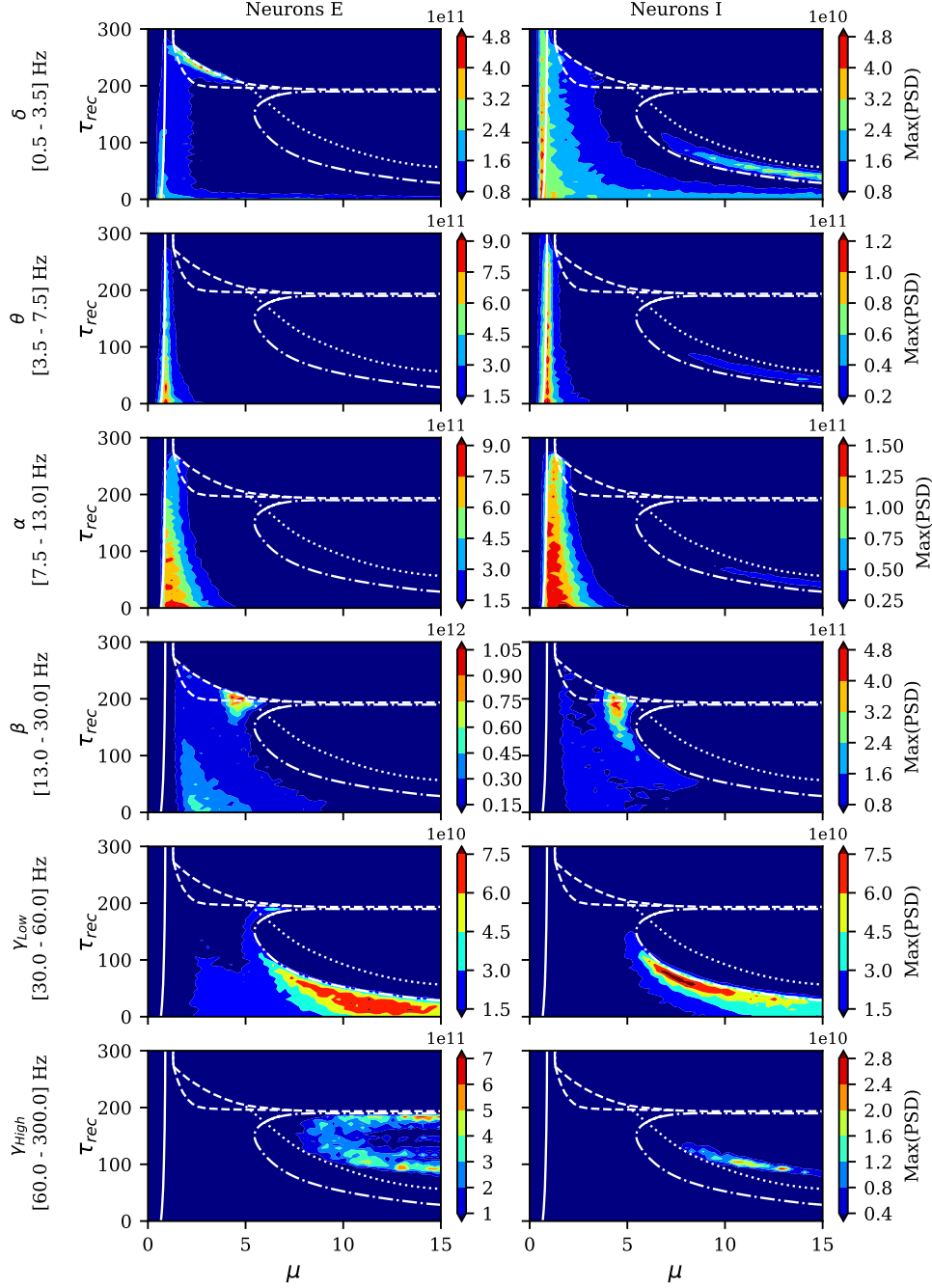


Figure S1: Maximum of power spectral density (PSD) by frequency bands across phase diagram. PSD calculated from the average membrane potential of a group of E and I neurons, following the macro-scheme explained in Figure ?? of the main text. The dotted(dash-dotted) line indicates the maximum variance of the excitatory (inhibitory) neurons state (see Figure ?? main text). The solid(dashed) white lines indicate a second-order (first-order) phase transition. Low frequencies dominate in the low noise region after the second-order transition takes place; however, excitatory δ waves are strongest close to the first order transition in the meta-stable region (between white dashed lines). β waves are also stronger in the metastable region for higher noise values, but extend their dominance in the low intermediate activity region below the metastable region. γ_{Low} dominates the high-noise and low τ_r region, close to the maximum variance of inhibitory neuron states X . Finally, high frequencies emerge in the E-I high-activity region (region enclosed by the dotted curve). High-frequency waves (γ_{High}) have a complex pattern similar to that observed for the variance of inhibitory activity, indicating that these rhythms are caused by complex activity in the inhibitory population

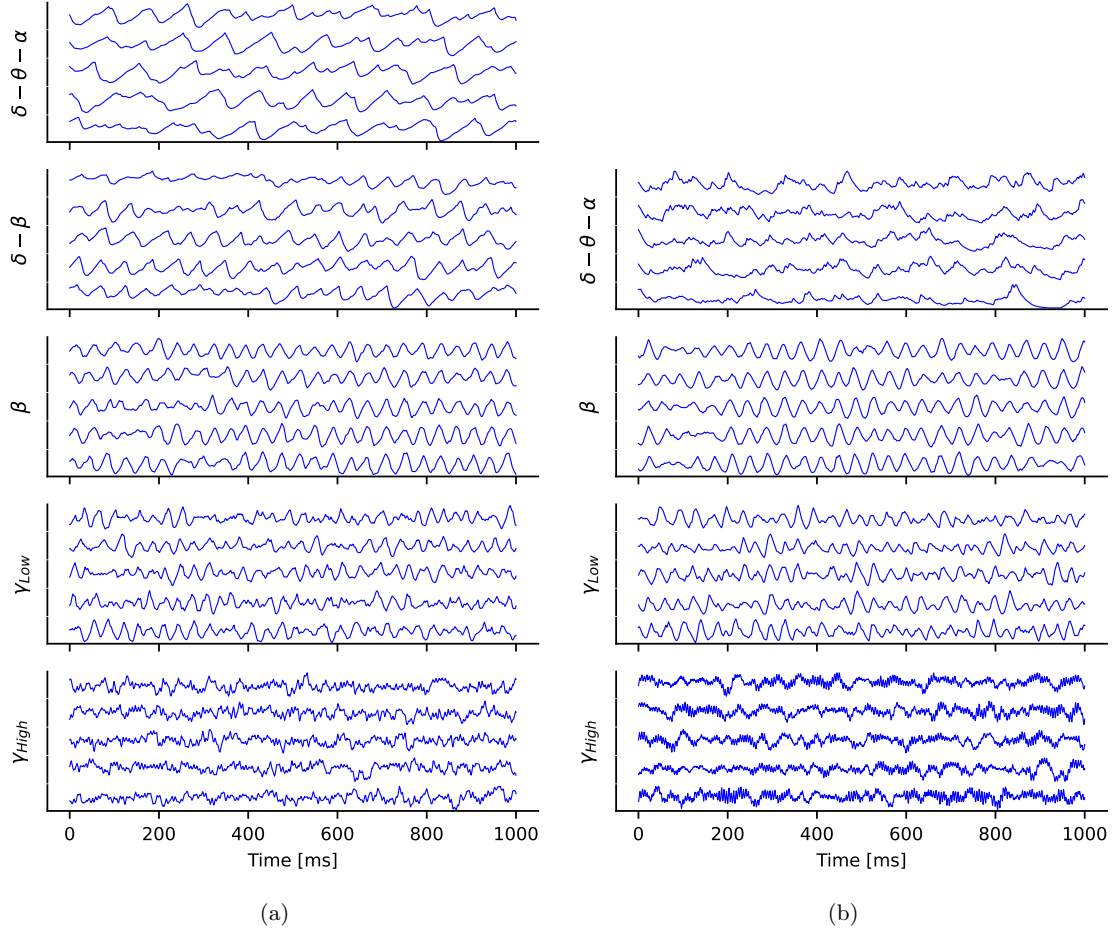
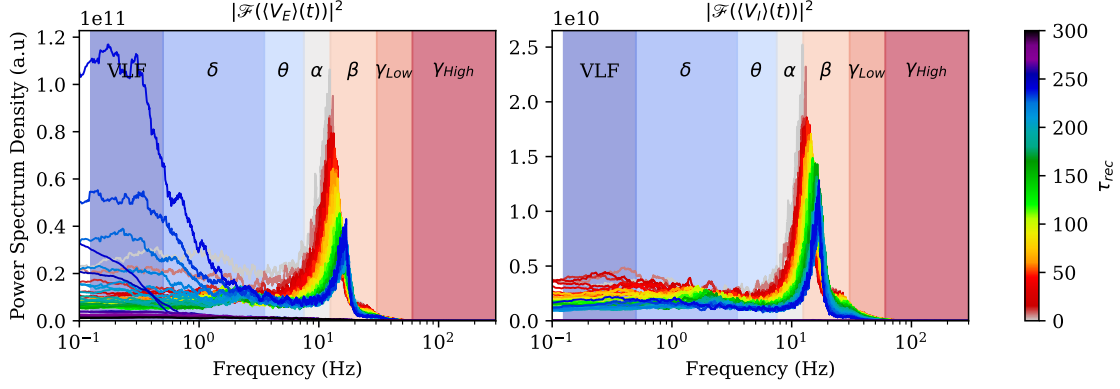
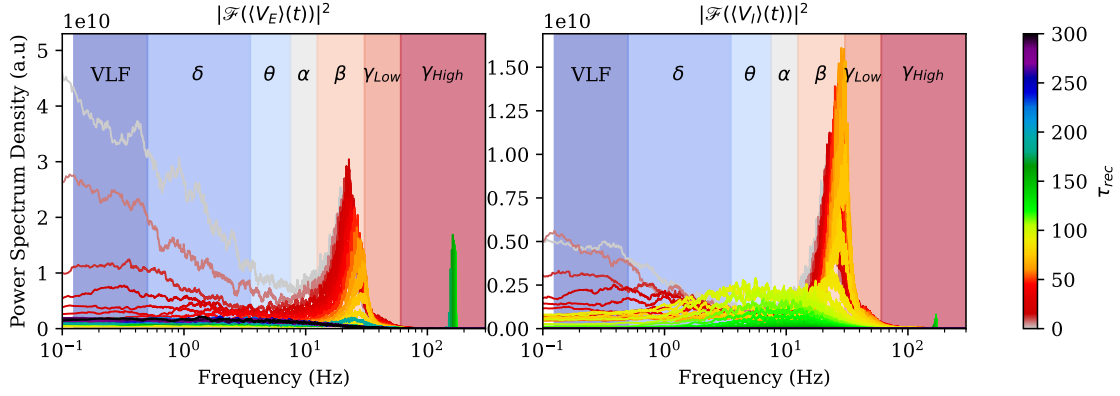


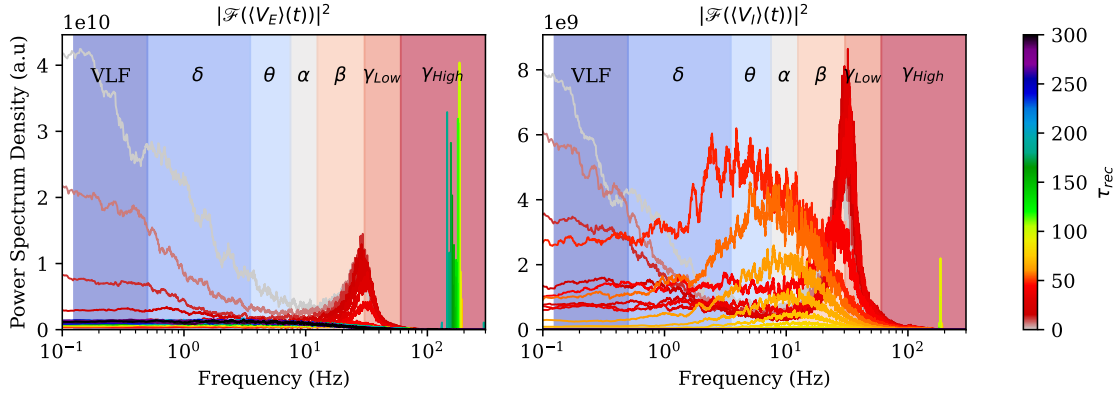
Figure S2: **Average membrane potential of 5 groups of neurons in different points of parameter (μ, τ_{rec}) space.** (a) Average excitatory membrane potential. (b) Average inhibitory membrane potential. Points used are shown as colored starts in Fig.?? and Fig.?. y-axis label indicates which rhythms are superposed in the selected point. The 5 groups correspond to the macro-scheme presented in Fig.??.



(a) Fixed $\mu = 2.449$



(b) Fixed $\mu = 7.653$



(c) Fixed $\mu = 12.551$

Figure S3: PSD of $\langle V \rangle$ in a group of neurons vs τ_{rec} for fixed values of μ . Colored areas indicate the rhythm band frequency. (Left a-c) PSD of average excitatory membrane potential. (Right a-c) PSD of average inhibitory membrane potential. (a-c) Waves can be observed until the first-order phase transition. Wave frequency increases with increasing external noise. (c) γ waves have a narrow band, first appearing at $\tau_{rec} \approx 90$ ms. In excitatory neurons, the waves disappear between $140 \lesssim \tau_{rec} \lesssim 160$ ms, reappearing after 160 ms but with a lower frequency, probably caused by the reduction in the available synaptic resources as τ_{rec} increases. In the 9 inhibitory neuron group, the waves are noisy with increasing values of μ . This shows how inhibition stabilizes the activity in the excitatory population, but there is no stabilization in the I population, because the model does not include I-I connections.

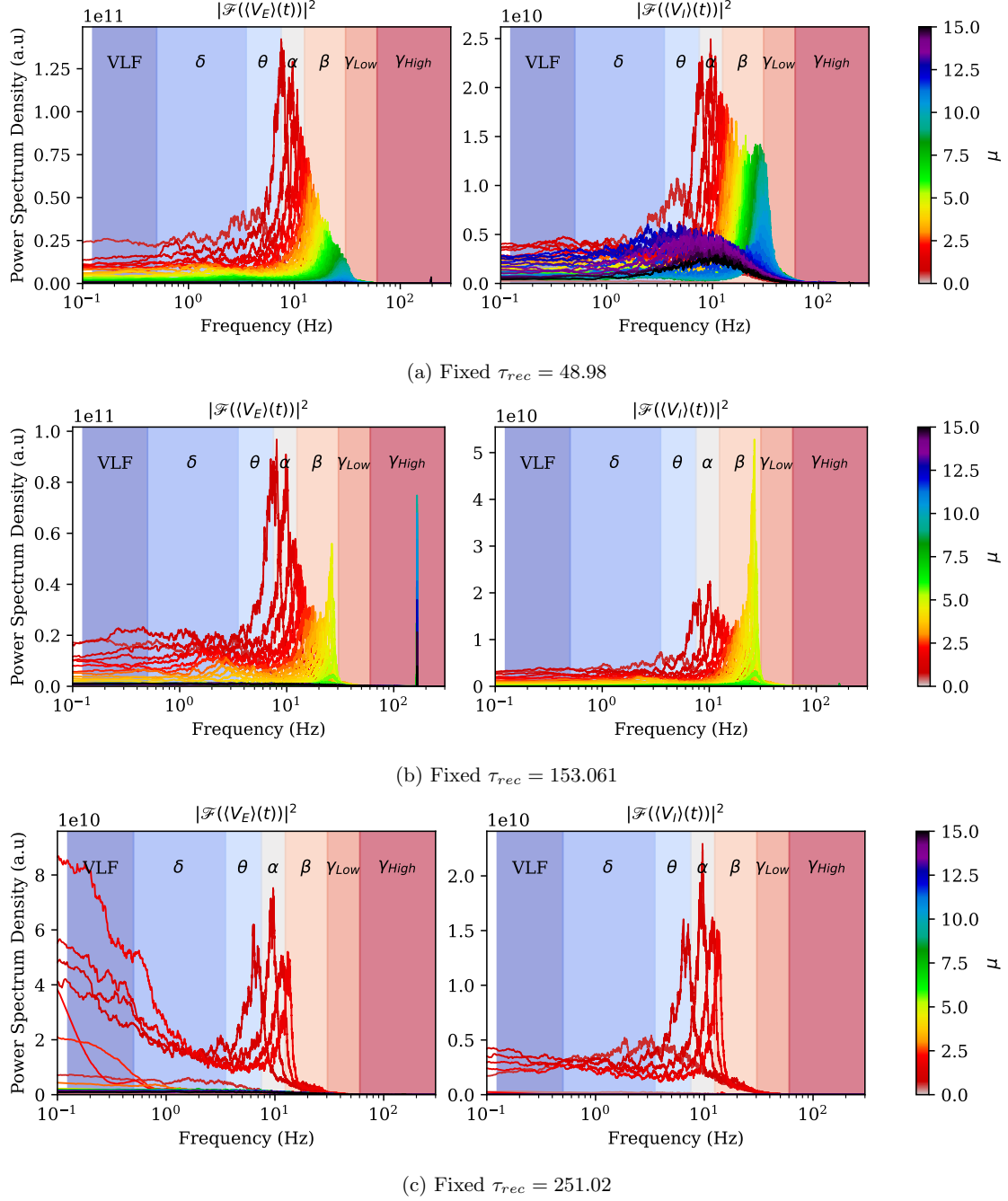


Figure S4: PSD of $\langle V \rangle$ in a group of neurons vs μ for fixed values of τ_{rec} . Colored areas indicate the rhythm band frequency. (Left a-c) PSD of average excitatory membrane potential. (Right a-c) PSD of average inhibitory membrane potential. (a) The amplitude of the waves decreases with increasing noise. (b) The amplitude first decreases with noise, but a peak of amplitude is observed for $2.5 < \mu < 5$ in the high β almost γ_{Low} . In the inhibitory population, this β peak is more dramatic, being almost 3 times larger than the amplitudes of other waves. (c) For $\tau_{rec} > 200$ ms, waves emerge only in a narrow band of μ values.

2 Phase diagram and rhythms

2.1 Excitatory and inhibitory activity

The phase diagram based on the neuronal activity of the system in the (μ, τ_{rec}) parameter space is shown in Figure S5.a. Three different regions are observed. First, with very low noise μ , to the left of the continuous transition (white solid line) we have a subcritical regime where both E and I neuron populations are inactive $\rho \approx 0$ (black region I). The second region (II) between the continuous phase transition and a discontinuous transition (white dashed line) is characterized by the fact that the E and I neuronal populations are both active, but they can be in different regimes: a low intermediate activity (II.a) and a high activity regime (II.b). Finally, we observe a third region (region III) after the discontinuous transition, where excitatory activity increases dramatically, while inhibitory activity dies off as the synaptic recovery time constant τ_{rec} is too large to allow an effective coupling between excitatory and inhibitory neurons.

We also measure the temporal variance of the activity of both neuronal populations (Figure S5.b). We found that excitatory populations have low variability in their activity, with the exception of a small region, whereas inhibitory populations show rich behavior in the high-activity region (II.b). This difference could be explained by the fact that excitatory activity is driven by the external noise and modulated/stabilized by inhibitory activity, while inhibitory activity depends only on excitatory activity and is not modulated, since I-I connections were not included. In future work, we will explore the impact of I-I and E-E connections in the activity fluctuations and in the information dynamics of this model.

In Figure S5.c, we observe the variance of the neuron states X instead of the temporal variance of neuronal activity ρ . We see that a maximum (gray region) occurs at the transition from low activity (II.a) to high activity (II.b), indicating that a phase transition that was not reported in the previous literature [? ?] could be taking place, a transition equivalent to the so-called low activity intermediate (LAI) phase transition [?].

In conclusion, from this analysis we observe that there is four characteristic regimes related to the network activity:

- I) An absorbing or silent regime for low external drive μ , which is almost independent on the time scale constant of the synaptic resources recovery τ_{rec} .
- II.a) A low activity intermediate region between the second order and first order transition lines, occurring for small to intermediate values of μ and τ_{rec} in both neuronal populations.
- II.b) A high activity region of both neuronal populations for high external noise μ and intermediate values of τ_{rec} ($50 \lesssim \tau_{rec} \leq 200$).
- III) After a critical value of τ_{rec} , the activity of the inhibitory population vanishes and a high excitatory activity driven by noise emerges.

Now we will explore the emergence of rhythms in the average membrane potential of excitatory and inhibitory neurons and relate them to the emerging phases described above.

3 Neural activity and emergence of γ_{High} oscillations.

Figures S6.b and S6.e show that there is no clear relation between excitatory activity and γ_{High} rhythms, since there are points where excitatory activity is high but no dominant peak is observed in PSD. However, there is a minimum inhibitory activity necessary for the occurrence of γ_{High} waves, since all points with $\max\{PSD\} > 10$ for excitatory and $\max\{PSD\} > 9$ for inhibitory have $\rho^I > 0.6$. Therefore, it is clear that the emergence of these rhythms in our system is linked with inhibitory activity, although increasing inhibitory activity does not explain well the increase in PSD peak, as can be seen in the same figures. In fact, the values with maximum inhibitory activity (red) appear to have a lower power (less than $\max\{PSD\} > 10^{11}$ for E and less than 2×10^9 for I), indicating a non-linear relationship between the emergence of γ_{High} and excitatory and inhibitory activity.

Finally, when observing the variance in neuronal activity (Figures S6.c), we see that the high excitatory γ rhythms are more dominant when inhibitory activity has a high temporal variance in a specific interval of inhibitory activity ($0.6 < \rho^I < 0.72$). On the contrary, the emergence of high inhibitory γ oscillations is not related to the temporal variance in excitatory activity in a similar way. As we can see in Figure S6.f, there is a set of points where the PSD peak increases even with decreasing variance

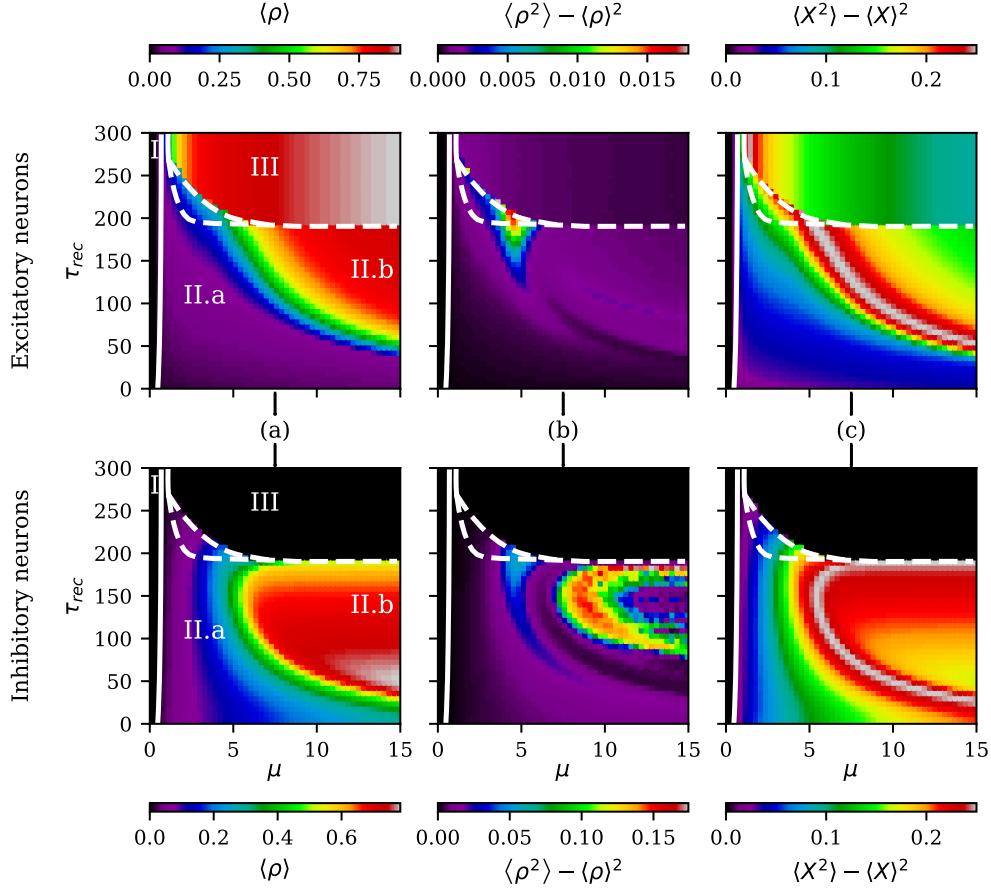


Figure S5: **Neuronal activity features across the (μ, τ_{rec}) parameter space.** The solid white line on the left shows the second-order phase transition from silent to active state (AT). The dashed white line shows the emergence of an explosive first-order transition. The region between dashed lines is the meta-stable phase. (a) Temporal average of excitatory and inhibitory neuronal activity: The region between the second-order and first-order transitions shows what appears to be a low activity intermediate phase (II.a), which gives place to a full active phase of high activity (II.b) for noise values $\mu > 5$. (b) Temporal variance of excitatory and inhibitory neuronal activity: The inhibitory population shows a complex activity pattern, whereas the excitatory population has low temporal variability in activity. (c) Temporal variance of Boolean states (X) of neurons: The maximum variance (gray region) appears to mark the transition line between the low activity intermediate phase and the high activity phase.

in excitatory activity. Therefore, only looking at the temporal variance of activity is not enough to understand the emergence of these rhythms.

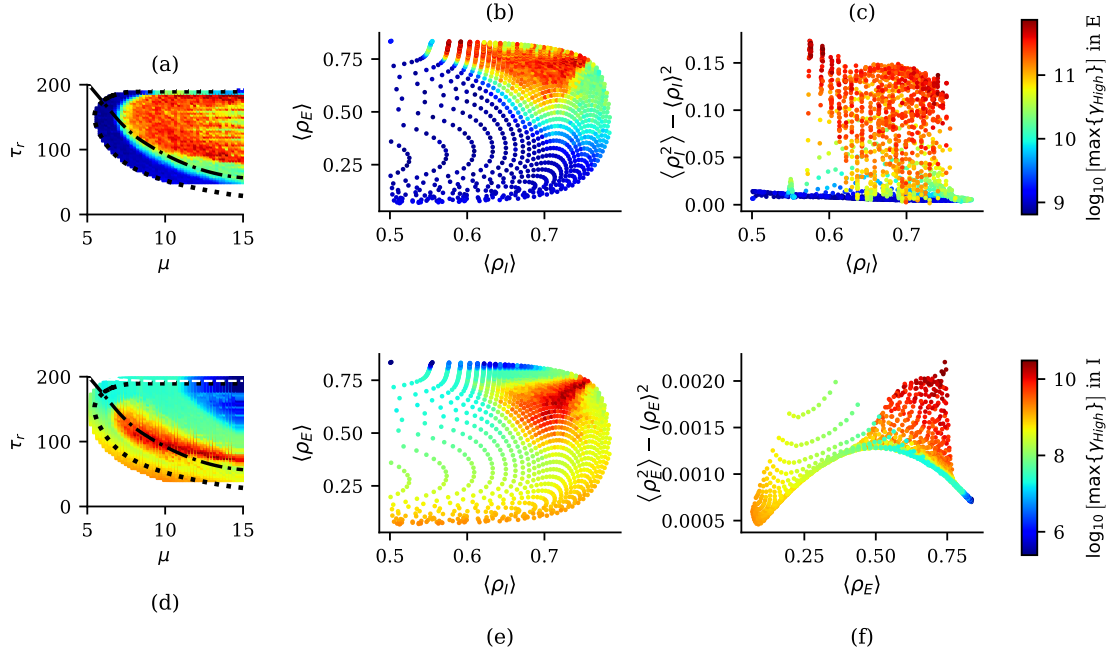


Figure S6: **Emergence of γ_{High} is related to the fluctuations in inhibitory activity.** (a,d) Heat maps: Excitatory (top, a-c) and inhibitory (bottom, d-f) peaks in PSD of the high γ band at points of the space parameter (μ, τ_{rec}) where $\rho_{E/I} > 0.5$ (inhibitory high activity phase). Panels (b, c) and (e, f) show the scatter plots of the points presented in (a) and (d), respectively. (b, e) Relation between mean neuronal activities and γ PSD peaks. Panels (c, f) show relations between the temporal variance of activity and the mean neuronal activity of one population with respect to oscillations in the other population. In (b) we observe that there is no direct relation between excitatory activity and the emergence of high frequency oscillations in this population; thus, the observed rhythm is not just an effect of the increasing excitatory firing rate caused by a random external input. Panel (c) illustrates that the power of high-frequency oscillations in the excitatory population increases with the variance in inhibitory activity. This suggests that in our system, excitatory γ_H rhythms are related to the interaction between excitatory activity and fluctuations in inhibitory activity. Panel (f) illustrates that the variance of excitatory activity also maps with higher power of inhibitory high-frequency oscillations, but with exceptions. A cloud of points of intermediate and high power emerges even with low excitatory activity and variance, suggesting a more complex relation between both.

4 Changes of information measures in time

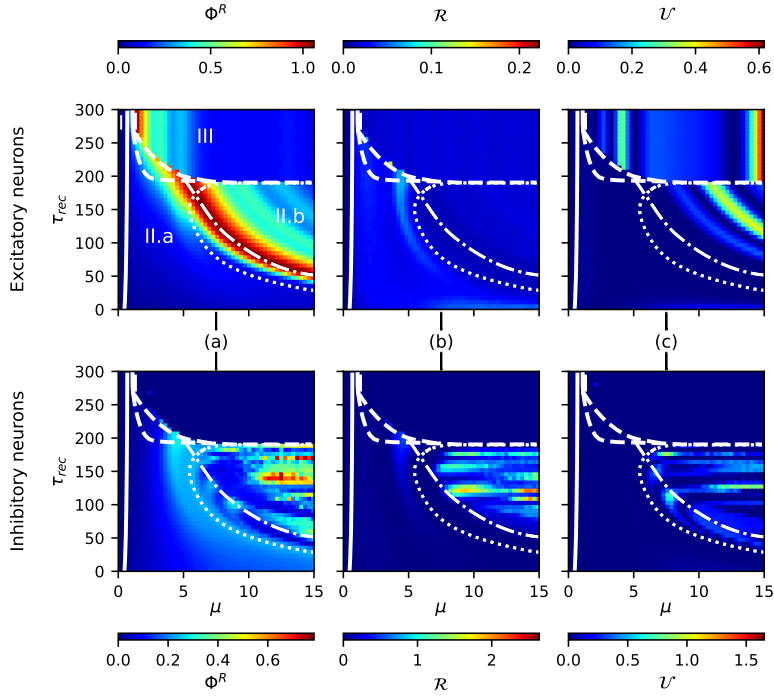


Figure S7: **Information measures** (Φ^R , \mathcal{R} , \mathcal{U}) for $\tau = 10$ time steps. (a) Integrated information in both excitatory and inhibitory group has the same behavior as that observed for time delayed $\tau = 1$, a maximum in the transition between LAI phase and high activity phase in excitatory population and spots of high integrated information in high inhibitory activity (see main text). (b-c) Redundant and Differentiated Information change considerably respect the measures done with $\tau = 1$. The differentiated information in excitatory population have clear bands of high and low values dependent on noise level, which could be the effect of the time delay used and the given firing rate induced by the noise level. An deep analysis of these effects will be carried in future work.

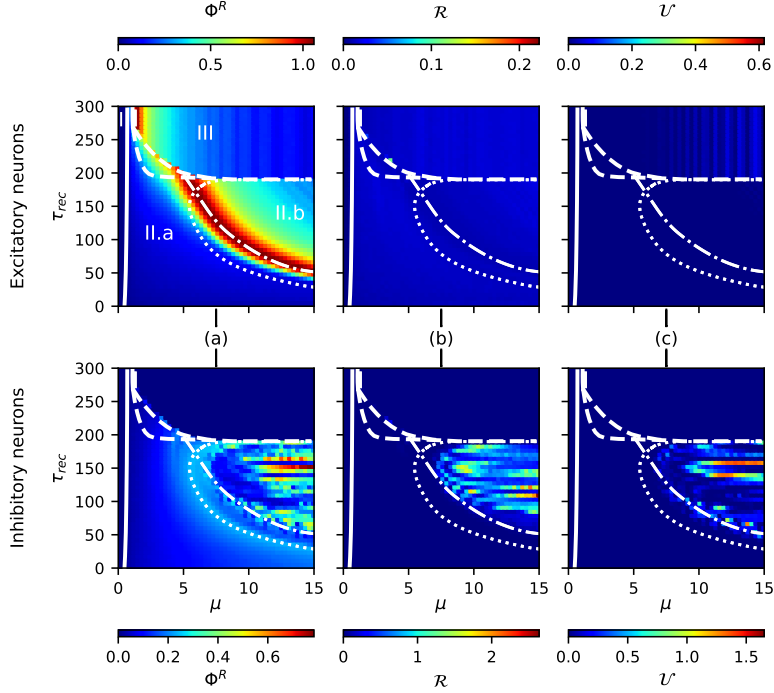


Figure S8: **Information measures** (Φ^R , \mathcal{R} , \mathcal{U}) for $\tau = 100$ **time steps**. Integrated information presents the same behavior as that observed for time delays $\tau = 1$ and $\tau = 10$. In the excitatory case, Φ^R seems time-invariant where it reaches maximum, which coincides with the maximum excitatory state variance line (dashed dotted white line) that marks the transition between the LAI phase and the high activity phase. (b-c) Redundancy and differentiation decrease considerably in the excitatory population compared to the measures for $\tau = 1$ and $\tau = 10$, while maintaining high values in the inhibitory high activity phase. The information dynamics in the inhibitory population shows patterns in the parameter space that have a complex dependence on the time delay τ . In the excitatory population, however, the information dynamics seems to generally decrease with time delay, with the exception of the region of transition, where Φ^R seems invariant with time.

5 Information dynamics and γ_{High} power spectrum

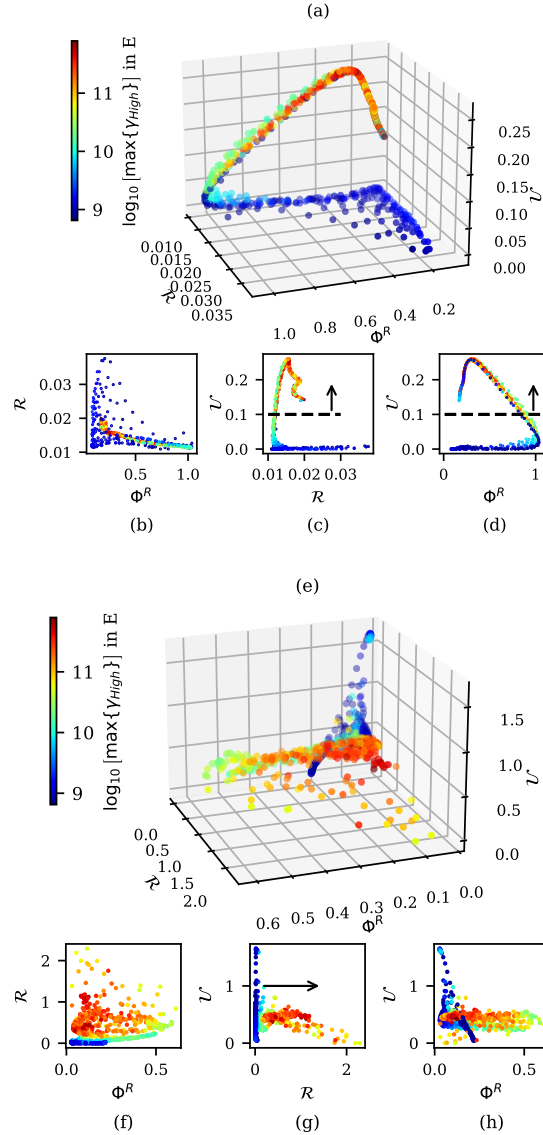


Figure S9: **Emergence of γ_{High} rhythms in E groups and the information dynamics of the system.** Colors indicate the intensity of the γ_{High} oscillation power. (a-d) Information dynamics of the excitatory group. (e-h) Information dynamics of the inhibitory group. γ_{High} is related to higher information differentiation (high \mathcal{U}) and low redundancy (low \mathcal{R}) in the excitatory group, indicated in (c, d) with a dashed line and arrow; however, there are exceptional points where we see a high \mathcal{U} but a weak γ power ($< 9 \times 10^{10}$). These exceptional points can be explained if we look at information dynamics in the inhibitory population, which modulates excitatory activity. Excitatory γ_{High} rhythms are related to a high redundancy in the inhibitory group, indicated by a black arrow in (g); therefore, even when some points have a high \mathcal{U} in the E group, they do not have high γ power due to low redundancy in the inhibitory population.

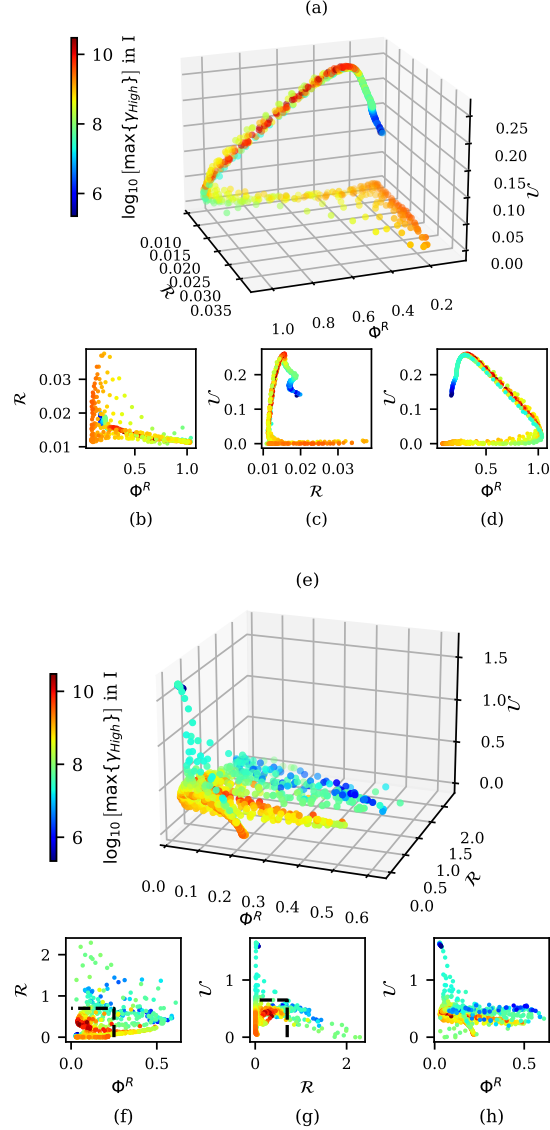


Figure S10: **Emergence of γ_{High} rhythms in I groups and the information dynamics of the system.** Colors indicate the intensity of the γ_{High} oscillation power in the inhibitory group. (a-d) Information dynamics of the excitatory group. (e-h) Information dynamics of the inhibitory group. γ_{High} does not have a clear relation with the information dynamics in the excitatory group, as points with high γ power are dispersed across our information dynamics space (\mathcal{R} , Φ^R , \mathcal{U}). However, looking at the dynamics of information in the inhibitory group, we observe that inhibitory high γ oscillations occur when we have low total information, as points with high γ power are concentrated closer to the point (0,0,0), indicated with dashed black line in (f) and (g).